

# Neutrino Mass Measurement with Cosmic Gravitational Focusing

Shao-Feng Ge <sup>\*1,2</sup>, Pedro Pasquini <sup>†3</sup>, and Liang Tan <sup>‡1,2</sup>

<sup>1</sup>Tsung-Dao Lee Institute & School of Physics and Astronomy, Shanghai Jiao Tong University, Shanghai 200240, China

<sup>2</sup>Key Laboratory for Particle Astrophysics and Cosmology (MOE) & Shanghai Key Laboratory for Particle Physics and Cosmology, Shanghai Jiao Tong University, Shanghai 200240, China

<sup>3</sup>Department of Physics, University of Tokyo, Bunkyo-ku, Tokyo 113-0033, Japan

July 8, 2024

## Abstract

We thoroughly explore the cosmic gravitational focusing of cosmic neutrino fluid (C $\nu$ F) by dark matter (DM) halo using both general relativity for a point source of gravitational potential and Boltzmann equations for continuous overdensities. Derived in the general way for both relativistic and non-relativistic neutrinos, our results show that the effect has fourth power dependence on the neutrino mass and temperature. With nonlinear mass dependence which is different from the cosmic microwave background (CMB) and large scale structure (LSS) observations, the cosmic gravitational focusing can provide an independent cosmological way of measuring the neutrino mass and ordering. We take DESI as an example to illustrate that the projected sensitivity as well as its synergy with existing terrestrial neutrino oscillation experiments and other cosmological observations can significantly improve the neutrino mass measurement.

---

\*gesf@sjtu.edu.cn

†pedrosimpas@g.ecc.u-tokyo.ac.jp

‡tanliang@sjtu.edu.cn

# 1. Introduction

When Pauli proposed neutrino to explain the continuous  $\beta$  decay spectrum in 1931, he also argued in the same famous letter that neutrino mass should be no greater than 1% of the proton mass [1]. Otherwise, the final-state electron spectrum should have apparent distortion around its endpoint [2]. This feature can be used to measure the absolute neutrino masses [2–4] such as at the ongoing KATRIN experiment [5]. However, the  $\beta$  decay endpoint measurement is sensitive to the neutrino mass combination  $m_\beta \equiv \sqrt{\sum_i |U_{ei}|^2 m_i^2}$  [6] where  $U_{\alpha i}$  is the PMNS matrix element [7]. While the current limits are  $m_\beta < 0.8$  eV at 90% C.L. [6], the future sensitivity can reach  $m_\beta \lesssim 0.2$  eV [8].

Probably out of Pauli’s expectation, not just the neutrino itself but also its mass plays very important roles in particle physics and cosmology. As first established by atmospheric [9] and solar [10] neutrino oscillation experiments, neutrinos have non-zero mass squared differences  $\Delta m_{ij}^2 \equiv m_i^2 - m_j^2$  [4]. The nonzero neutrino mass is the first experimentally verified new physics beyond the Standard Model of particle physics. Whether it is a genuine mass or just environmental effect due to scalar [11] and dark [12–15] non-standard interactions via forward scatterings needs further experimental identification. However, the neutrino oscillation cannot measure the absolute neutrino mass. The current global fits [16–18] of neutrino oscillation experimental data give  $\Delta m_s^2 \equiv \Delta m_{21}^2 \approx 7.54 \times 10^{-5}$  eV<sup>2</sup> and  $|\Delta m_a^2 \equiv \Delta m_{31}^2| \approx 2.47 \times 10^{-3}$  eV<sup>2</sup> [7]. Note that the sign of  $\Delta m_a^2$  is currently unknown which means the neutrino masses can be either normal ordering (NO) if  $\Delta m_a^2 > 0$  with  $m_1 < m_2 < m_3$  or inverted ordering (IO) if  $\Delta m_a^2 < 0$  with  $m_3 < m_1 < m_2$ . By 2030, the JUNO experiment [19,20] will determine the mass ordering [21–28] with a  $3\sigma$  level of accuracy and can further improve to  $4\sigma$  by also including the atmospheric neutrino oscillation [29].

The neutrinoless double beta decay ( $0\nu 2\beta$ ),  $\mathcal{N}(A, Z) \rightarrow \mathcal{N}(A, Z + 2) + 2e^-$  [30], is another type of terrestrial experiment to measure neutrino mass if neutrinos are Majorana particles [31, 32]. Its half-life is proportional to the neutrino mass combination  $m_{ee} \equiv \sum_i m_i U_{ei}^2$ . Currently, the best upper bounds come from Kamdland-ZEN [33] and GERDA [34],

$$|m_{ee}| \leq 6.1 \times 10^{-2} \text{ to } 1.65 \times 10^{-1} \text{ eV} \quad \text{and} \quad |m_{ee}| \leq 7.9 \times 10^{-2} \text{ to } 1.8 \times 10^{-1} \text{ eV}, \quad (1.1)$$

at 90% C.L. However, the effective mass  $m_{ee}$  may be less than  $10^{-3}$  eV in the NO which is known as the funnel region. Although it seems like the funnel region means null observation and hence is experimentally unattractive, it allows pinning down the absolute neutrino mass in the range of (2 ~ 6) meV [35], simultaneously measuring the two Majorana CP phases [36,37], and verifying whether there is LMA-Dark solution [38].

For the cosmic neutrino background (C $\nu$ B), its momentum around only 1.9 K is roughly the same size as the current temperature of our Universe [39] and could be smaller than the neutrino masses. Consequently, the neutrino mass can dominate the kinematics of C $\nu$ B which allows the possibility of distinguishing the Dirac and Majorana nature by a factor of 2 [40].

In addition, the PTOLEMY experiment [41–43] aims at measuring the emitted electron when capturing the cosmic relic neutrinos,  $\nu_e + {}^3\text{H} \rightarrow e^- + {}^3\text{He}$ . While the peak heights are determined by the mixing matrix elements, the peak locations of the electron energy corresponds to the neutrino mass eigenvalues [43]. If the electron energy resolution can be significantly improved, it is possible to use  $C\nu\text{B}$  for measuring the neutrino masses. Most notably, the tiny mass can induce a factor of 2 difference for  $C\nu\text{B}$  measurement via chiral oscillation [44, 45].

Another phenomena that can measure neutrino mass is the radiative emission of neutrino pair (RENP) [46–49]. With both superradiance and macroscopic coherent material, the RENP process that is induced by weak interactions can be significantly enhanced [50, 51]. Since the typical energy of atomic transitions is intrinsically at the  $\mathcal{O}(\text{eV})$  scale, RENP can be sensitive to not just light/massless mediators [52–54] but also those properties that are attached to the neutrino mass terms [55, 56]. In particular, the  $(10^{-3} \sim 10^{-2}) \text{eV}$  neutrino mass eigenvalues can leave a visible effect in the associated photon spectrum and hence can be measured by RENP [57, 58].

In addition to those terrestrial neutrino experiments mentioned above, astrophysical observations can also use the flight time delay of neutrinos from a nearby supernova to measure the neutrino mass [59]. Massive neutrinos propagate slower than the speed of light and hence experience flight time delay comparing with the massless photon. This time delay depends on the neutrino mass squared  $m_\nu^2$ ,  $\Delta t = 0.005 \text{ s} \times (D/10 \text{ kpc}) \times (m_\nu[\text{eV}]/E_\nu[10\text{MeV}])^2$  [59, 60], where  $D$  is distance and  $E_\nu$  the neutrino energy. The observation of a few neutrino events from SN1897A has led to the neutrino mass bound  $m_\nu < 5.7 \text{ eV}$  at 95% C.L. [61]. With the expectation of detecting several hundreds of supernova neutrino events in the future, the neutrino mass limits can be pushed to  $m_\nu \lesssim 1 \text{ eV}$  [60, 62, 63].

Cosmology is by far the most promising way to measure the neutrino masses [64, 65]. Neutrinos are ultra-relativistic when decoupling from the thermal bath with temperature  $\sim 1 \text{ MeV}$  [66]. As the temperature drops, massive neutrinos become non-relativistic [66]. The non-relativistic neutrino decreases CMB power spectrum due to less ISW effect and suppress matter power spectrum due to the neutrino free-streaming [7]. Both CMB and LSS observations are sensitive to the neutrino energy density  $\rho_\nu \equiv \sum n_\nu m_i \approx n_\nu \sum m_i$  that is a product of the neutrino number density  $n_\nu$  of a single species ( $\nu_i$  and  $\bar{\nu}_i$ ) and the neutrino mass sum  $\sum m_i$ . The combination of the Planck 2018 [67] and DES results [68] puts the most stringent constraint,  $\sum m_i < 0.13 \text{ eV}$  at 95% C.L. [7, 68]. Also, neutrino clustering can bend the background photon to induce a dipole structure in CMB [69, 70]. Similarly, the neutrino gravitational focusing effect by DM halo can also be probed by the galaxy weak lensing observation [71]. These two effects are sensitive to the neutrino masses.

In addition to the standard cosmology approaches, we explore an additional and independent method for measuring neutrino masses based on the cosmic gravitational focusing between the  $C\nu\text{F}$  and dark matter halos [72–75]. With dependence on the mass fourth power instead of

the usual linear neutrino mass sum, the cosmic gravitational focusing is more sensitive to the neutrino masses and can provide a complementary measurement. Such an effect can be measured by the two-point and three-point galaxy correlation observations at the coming next generation of galaxy surveys. Especially, the Dark Energy Spectroscopic Instrument (DESI) [76, 77] has already started the data release [78], Euclid was launched on July 2023 [79], and CSST (China Space Station Telescope) will be launched around 2024 or so [80–82]. We will show the projected sensitivity by taking DESI for illustration.

This paper is organized as follows. We introduce the formalism for the focusing of  $C\nu F$  in the gravitational potential of DM halo Sec. 2 for both non-relativistic and relativistic neutrinos. In Sec. 3, we calculate the galaxy correlation observables and the signal-to-noise ratio (SNR). Finally in Sec. 5, we simulate the expected DESI sensitivity to the neutrino mass with the galaxy categories summarized in Sec. 4 for illustration. Our conclusion can be found in Sec. 6.

## 2. Cosmic Gravitational Focusing

When a flow of collisionless particles pass by a massive object, they can experience gravitational lensing [83–85]. With an attractive gravitational force, particles with the same incoming velocity are bent towards each other and focus behind the massive object to enhance the density there. Such gravitational focusing effect can leave detectable annual modulation in the direct detection of DM with our Sun being the massive object to provide gravitational source [86–89]. Since DM contributes the most to the matter world in our Universe, cosmic gravitational focusing of  $C\nu F$  under the influence of DM halo happens more vastly. The  $C\nu F$  density increase by the gravitational focusing will generate a dipole density distribution around the central DM halo which subsequently affects the galaxy density distribution that can be observed via the galaxy cross correlation.

We first derive the general expressions of cosmic gravitational focusing with a single DM halo as a point source of gravitation force in Sec. 2.1. Especially, we reproduce the dependence of drag force on the fourth power of neutrino masses with non-relativistic speed. However, our results apply more generally for relativistic neutrino fluids with temperature dependence. To overcome the intrinsic logarithmic divergence in this point-source approach, we further adapt the Boltzmann equation formalism in Sec. 2.2 which can apply more generally.

### 2.1. The Trajectory and Drag Force Formalism

In addition to gravitational focusing, gravitational lensing can also lead to dynamical friction [90] which plays important roles in astrophysics, such as the formation of planets [91], star clusters [92], and galaxies [93]. So the cosmic gravitational focusing of  $C\nu F$  under the influence of DM halo is also called as dynamical friction [72]. Below we first provide a classical picture of

single-particle trajectory and its deflection to derive the drag force which is an essential feature of dynamical friction.

When an object moves through a bunch of collisionless particles, its gravitational force can deflect the originally free moving particles. To give an intuitive picture, let us first consider a single neutrino passing by a DM halo with mass  $M$ . In the spherical coordinate  $(t, r, \theta, \phi)$  with DM halo at its origin, the space-time can be described by,

$$ds^2 \equiv - \left(1 - \frac{2GM}{r}\right) dt^2 + \left(1 - \frac{2GM}{r}\right)^{-1} dr^2 + r^2 d\Omega^2, \quad (2.1)$$

where  $G$  is the Newton constant and  $d\Omega$  the solid angle element. One may see that the effect of the DM halo gravitational potential appears in front of  $dt^2$  and  $dr^2$ . A free moving neutrino follows the geodesic equation that has four constants of motion,

$$\left(1 - \frac{2GM}{r}\right) \frac{dt}{d\tau} \equiv C_t, \quad r^2 \frac{d\theta}{d\tau} \equiv C_\theta, \quad r^2 \sin^2 \theta \frac{d\phi}{d\tau} \equiv C_\phi, \quad (2.2a)$$

$$\left(1 - \frac{2GM}{r}\right)^{-1} \left(\frac{dr}{d\tau}\right)^2 - \left(1 - \frac{2GM}{r}\right)^{-1} C_t^2 + \frac{C_\phi^2}{r^2} \equiv C_r, \quad (2.2b)$$

where  $\tau$  is the proper time. The integration constants  $C_t$ ,  $C_r$ ,  $C_\theta$ , and  $C_\phi$  are determined by initial conditions. Due to reflection symmetry, one may reduce the three-dimensional coordinate to a two-dimensional one where the neutrino trajectory resides on the  $x-y$  plane with  $z$  always being 0. This means the zenith angle is fixed with  $\theta = \pi/2$  and  $C_\theta = 0$ . In addition to time  $t$ , both the radius  $r$  and azimuthal angle  $\phi$  can vary. Taking the radius  $r$  to infinity,  $r \rightarrow \infty$ , the metric approaches a free particle and we can identify  $C_t = \sqrt{m_\nu^2 + |\mathbf{p}_i|^2}/m_\nu \equiv E_i/m_\nu$ ,  $C_\phi = E_i |\mathbf{b}| |\mathbf{v}_i|/m_\nu$ , and  $C_r = -1$ , where  $\mathbf{b}$  is the impact parameter and  $\mathbf{v}_i \equiv \mathbf{p}_i/E_i$  is the neutrino initial velocity.

Combining the equations for  $\phi$  and  $r$  in Eq. (2.2) with the relation  $d\phi/dr = d\phi/d\tau (dr/d\tau)^{-1}$ , we obtain the total deflection angle of the neutrino when passing by the DM halo,

$$\Delta\phi = 2|\mathbf{b}| \int_{r_{\min}}^{\infty} \frac{dr}{r^2} \left[ 1 + \frac{2b_{90}}{r} - \frac{|\mathbf{b}|^2}{r^2} + \frac{2GM|\mathbf{b}|^2}{r^3} \right]^{-1/2}. \quad (2.3)$$

Note that  $b_{90} \equiv GMm_\nu^2/|\mathbf{p}_i|^2$  denotes the impact parameter that corresponds to a  $90^\circ$  deflection of the neutrino momentum. Given impact parameter  $|\mathbf{b}|$ , the closest distance between neutrino and the central DM halo is  $r_{\min}$  as solution of  $r_{\min}^3 + 2b_{90}r_{\min}^2 - |\mathbf{b}|^2 r_{\min} + 2GM|\mathbf{b}|^2 = 0$ . For the large impact parameter approximation,  $|\mathbf{b}| \gg b_{90}$  and  $GM$ , the total deflection angle between the initial and final neutrino position vectors can be perturbatively expanded as,

$$\Delta\phi \approx \pi + 2 \frac{GM}{|\mathbf{b}|} \left( \frac{m_\nu^2}{|\mathbf{p}_i|^2} + 2 \right). \quad (2.4)$$

The deflection angle of the neutrino momentum corresponds to  $\Delta\phi - \pi$ . We take the  $x$ -direction anti-parallel to the initial neutrino velocity in the DM frame. Then, the initial  $\hat{\mathbf{p}}_i$  has  $\phi_i = \pi$  with direction  $\hat{\mathbf{p}}_i = -\hat{\mathbf{x}}$  while the final momentum  $\mathbf{p}_f \equiv |\mathbf{p}_i|(\cos \phi_f \hat{\mathbf{x}} + \sin \phi_f \hat{\mathbf{y}})$  has  $\phi_f = \Delta\phi$ .

We consider a stream of neutrinos whose phase space distribution  $f(\mathbf{p})$  is spatially independent. In other words, for any neutrino with certain momentum and impact parameter  $\mathbf{b}$  to pass by a DM halo, there is equal chance for a neutrino with the same momentum but opposite impact parameter  $-\mathbf{b}$ . Such a pair of neutrinos would experience equal amount of bending by the DM halo gravitational potential in opposite directions. In total, their total momentum along the initial one ( $\hat{\mathbf{p}}_f = -\hat{\mathbf{x}}$ ) is reduced while no total perpendicular (transverse) component can develop. The average momentum transfer is parallel to the  $x$ -direction and can be obtained from Eq. (2.4) as,

$$\Delta\mathbf{p}^{\parallel} \equiv \mathbf{p}_f^{\parallel} - \mathbf{p}_i = (-\cos\Delta\phi - 1)\mathbf{p}_i \approx -\frac{2G^2M^2}{|\mathbf{b}|^2} \left( \frac{m_\nu^2}{|\mathbf{p}_i|^2} + 2 \right)^2 \mathbf{p}_i. \quad (2.5)$$

To calculate the drag force, let us consider a bulk of neutrino with roughly the same initial velocity  $\mathbf{v}_i$  (equivalently momentum  $\mathbf{p}_i$ ) and magnitude of impact parameter  $|\mathbf{b}|$ ,

$$dN = (2\pi|\mathbf{b}|d|\mathbf{b}|)(|\mathbf{v}_i|\Delta t)dn_{\mathbf{p}_i}. \quad (2.6)$$

The first parenthesis  $2\pi|\mathbf{b}|d|\mathbf{b}|$  gives the cross section around the impact parameter  $|\mathbf{b}|$  while the second  $|\mathbf{v}_i|\Delta t$  is the distance traveled by neutrinos within the time during  $\Delta t$ . Together, the product of volume  $dV \equiv (2\pi|\mathbf{b}|d|\mathbf{b}|)(|\mathbf{v}_i|\Delta t)$  and the particle number density  $dn_{\mathbf{p}_i} \equiv f_\nu(\mathbf{p}_i)d^3\mathbf{p}_i/(2\pi)^3$  in the momentum volume  $d^3\mathbf{p}_i$  gives the particle number  $dN$ .

The drag force on DM halo is then an integration of  $\Delta\mathbf{p}^{\parallel}/\Delta t$  over  $d|\mathbf{b}|$  and  $d^3\mathbf{p}_i \equiv |\mathbf{p}_i|^2d|\mathbf{p}_i|d\Omega_{\mathbf{p}_i}$ ,

$$\mathbf{F}_{\text{drag}} \equiv \int \frac{\Delta\mathbf{p}^{\parallel}}{\Delta t} dN = \frac{2}{\pi} \int \frac{G^2M^2d|\mathbf{b}|}{|\mathbf{b}|} \int \frac{d|\mathbf{p}_i|}{E_{\mathbf{p}_i}} (m_\nu^2 + 2|\mathbf{p}_i|^2)^2 \int \frac{d\Omega_{\mathbf{p}_i}}{4\pi} f_\nu(\mathbf{p}_i)\hat{\mathbf{p}}_i, \quad (2.7)$$

where the neutrino velocity  $|\mathbf{v}_i|$  in Eq. (2.6) has been replaced by  $|\mathbf{p}_i|/E_{\mathbf{p}_i}$ . For clarity, the integration has been divided into three parts for the impact parameter  $d|\mathbf{b}|$ , the neutrino momentum  $d|\mathbf{p}_i|$ , and the neutrino direction  $d\Omega_{\mathbf{p}_i}$ . If there is no relative velocity between the CνF and DM halo, the neutrino phase space distribution is isotopic,  $f_\nu(\mathbf{p}_i) = f_\nu(|\mathbf{p}_i|)$ , and consequently there is no dynamical friction. In other words, the dynamical friction comes from a nonzero relative velocity  $\mathbf{v}_{\nu c}$  or equivalently an anisotropic phase space distribution.

Starting with the Fermi-Dirac phase space distribution in the CνF frame,  $f_\nu(\mathbf{p}') = 2/(e^{|\mathbf{p}'|/T} + 1)$  including both the neutrino and antineutrino contributions, we perform a Lorentz boost to the DM halo frame. Since the relative velocity between the two frames is small  $|\mathbf{v}_{\nu c}| \sim \mathcal{O}(10^{-3})$  [72] as elaborated in App. A, the Lorentz boost can be expanded to the linear order of  $\mathbf{v}_{\nu c}$ ,  $\mathbf{p}' \approx \mathbf{p}_i - E_{\mathbf{p}_i}\mathbf{v}_{\nu c}$ . Consequently, the neutrino phase space distribution becomes,

$$f_\nu(\mathbf{p}_i, \mathbf{v}) \approx \frac{2}{e^{|\mathbf{p}_i - E_{\mathbf{p}_i}\mathbf{v}_{\nu c}|/T} + 1}. \quad (2.8)$$

Together with Eq. (2.7), the drag force is also linearly proportional to  $\mathbf{v}_{\nu c}$ ,

$$\mathbf{F}_{\text{drag}} = \frac{2\mathbf{v}_{\nu c}G^2}{3\pi} \left( m_\nu^4 + \frac{4\pi^2}{3}m_\nu^2T_\nu^2 + \frac{28\pi^4}{15}T_\nu^4 \right) \int M^2(<|\mathbf{b}|) \frac{d|\mathbf{b}|}{|\mathbf{b}|}. \quad (2.9)$$

For non-relativistic neutrinos,  $m_\nu \gg T_\nu$ , the drag force is proportional to the fourth power of the neutrino mass  $m_\nu^4$  which is a unique feature of the effect [73]. For the relativistic case,  $m_\nu \ll T_\nu$ , the drag force is proportional to the fourth power of its temperature  $T_\nu^4$ . This means that even massless neutrinos can induce a nonzero drag force on a DM halo.

However, the classical trajectory and force description summarized here has intrinsic flaws. When the impact parameter  $\mathbf{b}$  goes to infinity or zero, the integration receives logarithmic divergence [73]. Although the zero limit can be naturally avoided since the DM halo mass distribution  $M(< |\mathbf{b}|)$  is not a point source but instead has extended geometry, the other limit  $|\mathbf{b}| \rightarrow \infty$  has intrinsic difficulty with a stationary gravitational potential which effectively treat the gravitational attraction as force at a distance. This is not true since the DM halo forms and develops together with the evolution of our Universe. In addition, the key factor that affects the observable galaxy cross correlation function as elaborated in the next section is actually the focused density rather than the drag force. So it is necessary to find a more appropriate description of the cosmic gravitational focusing effect.

## 2.2. The Boltzmann Equation Formalism

The evolution of DM halo and the large scale structure of the whole Universe can be naturally described by the Boltzmann equations. Although there is no geometric picture as clear as the trajectory and drag force formalism in the previous Sec. 2.1, the Boltzmann equation formalism better fits the continuous overdensity distribution and cosmic gravitational focusing. Intuitively thinking, when the  $C\nu F$  passes by a DM halo, the bending of their trajectories also changes the neutrino density distribution. In other words, the neutrino density distribution can also manifest the trajectory bending and drag force.

The evolution of the neutrino phase space distribution is described by the following Boltzmann equation,

$$\left\{ \partial_t + \frac{\mathbf{p} \cdot \nabla_{\mathbf{x}}}{aE_{\mathbf{p}}} - \left[ (H + \dot{\Phi})\mathbf{p} + \frac{E_{\mathbf{p}}}{a} \nabla_{\mathbf{x}} \Psi - \frac{|\mathbf{p}|^2 \nabla_{\mathbf{x}} \Phi - \mathbf{p}(\mathbf{p} \cdot \nabla_{\mathbf{x}} \Phi)}{aE_{\mathbf{p}}} \right] \cdot \nabla_{\mathbf{p}} \right\} f_\nu(\mathbf{x}, \mathbf{p}) = 0, \quad (2.10)$$

where the gravitational effect of the DM halo has been encapsulated in the gravitational potentials  $\Phi$  and  $\Psi$  as defined in the conformal-Newtonian gauge  $ds^2 = -(1 + 2\Psi)dt^2 + (1 + 2\Phi)a^2 d\mathbf{x}^2$  with  $a$  being the scale factor [39]. The second term originally has a coefficient  $1 - \Phi + \Psi$  that is approximately 1 since both  $\Phi$  and  $\Psi$  are negligibly small. For further simplicity, one may also neglect the anisotropic stress,  $\Phi = -\Psi$ . The neutrino energy  $E_{\mathbf{p}}$  is subject to the on-shell condition,  $E_{\mathbf{p}} = \sqrt{|\mathbf{p}|^2 + m_\nu^2}$ .

We consider the late stage of Universe evolution when the cosmic gravitational focusing of  $C\nu F$  under the influence of DM halo becomes important. For simplicity, the  $C\nu F$  has static phase space distribution,  $\partial_t f_\nu \approx 0$ , and the Hubble rate  $H$  does not play a major role at small scales. Comparing the Hubble parameter term and the second term in the same



bracket of Eq. (2.10), the above approximation happens at  $|\mathbf{p}|/m_\nu \gg H\Delta x$ , namely,  $\Delta x \ll 7.4 \text{ Mpc} (0.1 \text{ eV}/m_\nu)(1+z)^{-1/2}$  [73] which is exactly the scale for neutrino free streaming as explored in [75]. In addition, the DM halo gravitational potential also varies slowly with time,  $\dot{\Phi} \sim 0$ . The neutrino phase space distribution,  $f_\nu(\mathbf{x}, \mathbf{p})$ , is then described by the time-independent Boltzmann equation [39],

$$\left\{ \frac{1}{aE_p} \mathbf{p} \cdot \nabla_{\mathbf{x}} - \left[ \frac{E_p}{a} \nabla_{\mathbf{x}} \Psi + \frac{|\mathbf{p}|^2 \nabla_{\mathbf{x}} \Psi - \mathbf{p}(\mathbf{p} \cdot \nabla_{\mathbf{x}} \Psi)}{aE_p} \right] \cdot \nabla_{\mathbf{p}} \right\} f_\nu(\mathbf{x}, \mathbf{p}) = 0. \quad (2.11)$$

In [75], a more general derivation beyond the static Boltzmann approximation is provided.

To make the focusing effect more apparent, the neutrino phase-space distribution can be decomposed into an homogeneous part  $\bar{f}_\nu(\mathbf{p})$  plus a tiny deviation  $\delta f_\nu$ ,

$$f_\nu(\mathbf{x}, \mathbf{p}) \equiv \bar{f}_\nu(\mathbf{p}) + \delta f_\nu(\mathbf{x}, \mathbf{p}). \quad (2.12)$$

Putting the decomposition back into the Boltzmann equation Eq. (2.11), the deviation  $\delta f_\nu$  can be induced by its homogeneous counterpart  $\bar{f}_\nu$  in the Fourier space,

$$\delta \tilde{f}_\nu(\mathbf{k}, \mathbf{p}) = \tilde{\Psi}(\mathbf{k}) \left( \frac{m_\nu^2 + 2\mathbf{p}^2}{\mathbf{p} \cdot \mathbf{k}} \mathbf{k} - \mathbf{p} \right) \cdot \nabla_{\mathbf{p}} \bar{f}_\nu(\mathbf{p}). \quad (2.13)$$

The quantities with a tilde are the Fourier modes,  $\delta \tilde{f}_\nu(\mathbf{k}, \mathbf{p}) \equiv \int d^3 \mathbf{x} e^{-i\mathbf{k} \cdot \mathbf{x}} \delta f_\nu(\mathbf{x}, \mathbf{p})$ . We can see that the gravitational potential  $\tilde{\Psi}$  induces the inhomogeneous deviation  $\delta \tilde{f}_\nu$  which is proportional to  $\tilde{\Psi}$  at the leading order.

The neutrino energy density fluctuations are obtained by integrating  $\delta \tilde{f}$  over all possible neutrino momenta,

$$\delta \tilde{\rho}_\nu(\mathbf{k}) \equiv \int \frac{d^3 \mathbf{p}}{(2\pi)^3} E_p \delta \tilde{f}_\nu(\mathbf{k}, \mathbf{p}) = \tilde{\Psi}(\mathbf{k}) \int \frac{d^3 \mathbf{p}}{(2\pi)^3} E_p \left( \frac{m_\nu^2 + 2\mathbf{p}^2}{\mathbf{p} \cdot \mathbf{k}} \mathbf{k} - \mathbf{p} \right) \cdot \nabla_{\mathbf{p}} \bar{f}_\nu(\mathbf{p}). \quad (2.14)$$

If there is no relative velocity, the neutrino phase space distribution is isotropic, i.e.  $\bar{f}_\nu(\mathbf{p}) = \bar{f}_\nu(|\mathbf{p}|)$ . Then, the momentum gradient is proportional to the neutrino momentum,  $\nabla_{\mathbf{p}} \bar{f}_\nu(|\mathbf{p}|) \propto \mathbf{p}$ . Consequently, the wave number ( $\mathbf{k}$ ) dependence in the parenthesis disappears,  $\delta \tilde{\rho}_\nu(\mathbf{k}) \propto \tilde{\Psi}(\mathbf{k}) \int E_p^3 d^3 \mathbf{p}$ , and the only  $\mathbf{k}$  dependence follows the DM gravitational potential  $\tilde{\Psi}(\mathbf{k})$ . In other words, the neutrino density fluctuation  $\delta \tilde{\rho}_\nu$  should following the DM one if there is no relative velocity and there is no dipole density distribution on the upstream and downstream sides around the DM halo. In the presence of relative velocity, the cosmic gravitational focusing should lead to larger neutrino density on the downstream side.

### 2.2.1. Neutrino Density Anisotropy from the Relative Velocity

In the presence of relative velocity, the neutrinos deflected by a DM halo tend to accumulate downstream. As a result, the neutrino density fluctuation has an anisotropy,  $\delta \rho_\nu(\mathbf{x}) \neq \delta \rho_\nu(-\mathbf{x})$  along the relative velocity. Correspondingly, the neutrino density fluctuation in the



wave number space after Fourier transformation would possess a non-zero imaginary part, i.e.  $\text{Im}[\delta\tilde{\rho}_\nu(\mathbf{k})] \neq 0$ <sup>1</sup>.

To find the explicit form of  $\text{Im}[\delta\tilde{\rho}_\nu]$ , we use the anisotropic phase space distribution in Eq. (2.8) as  $\bar{f}_\nu = f(\mathbf{p}, \mathbf{v}_{\nu c})$  back into Eq. (2.14). With a nonrelativistic  $\mathbf{v}_{\nu c}$ , it is much more convenient to first expand the distribution function,  $f_\nu(\mathbf{p}, \mathbf{v}_{\nu c}) \approx 2/(e^{|\mathbf{p}|/T_\nu} + 1) + E_{\mathbf{p}} \hat{\mathbf{p}} \cdot \mathbf{v}_{\nu c} / T_\nu (1 + \cosh |\mathbf{p}|/T_\nu)$ . Consequently, the momentum gradient becomes,  $\nabla_{\mathbf{p}} \bar{f}_\nu \approx \hat{\mathbf{p}}' [1 - (\mathbf{v}_{\nu c} \cdot \hat{\mathbf{p}}') / E_{\mathbf{p}}'] d\bar{f}(|\mathbf{p}'|) / d|\mathbf{p}'|$ , by noticing that the neutrino distribution  $\bar{f}_\nu(|\mathbf{p}'|)$  depends only on the modulus of the variable  $\mathbf{p}' = \mathbf{p} - E_{\mathbf{p}} \mathbf{v}_{\nu c}$ . Then, Eq. (2.14) becomes,

$$\delta\tilde{\rho}_\nu(\mathbf{k}) = \tilde{\Psi}(\mathbf{k}) \int \frac{d^3\mathbf{p}}{(2\pi)^3} E_{\mathbf{p}} \left( \frac{m_\nu^2 + 2\mathbf{p}^2}{\mathbf{p} \cdot \mathbf{k}} \mathbf{k} \cdot \hat{\mathbf{p}}' - \mathbf{p} \cdot \hat{\mathbf{p}}' \right) \left( 1 - \frac{\mathbf{v}_{\nu c} \cdot \hat{\mathbf{p}}'}{E_{\mathbf{p}}'} \right) \frac{d\bar{f}_\nu(|\mathbf{p}'|)}{d|\mathbf{p}'|}. \quad (2.15)$$

Now, we shift the variable of integration by  $\mathbf{p} \rightarrow \mathbf{p}' + E_{\mathbf{p}} \mathbf{v}_{\nu c}$  to write Eq. (2.15) as,

$$\delta\tilde{\rho}_\nu(\mathbf{k}) \approx \tilde{\Psi} \int \frac{d^3\mathbf{p}'}{(2\pi)^3} \frac{d\bar{f}_\nu}{d|\mathbf{p}'|} \frac{E_{\mathbf{p}'}^3}{(\mathbf{p}' + E_{\mathbf{p}'} \mathbf{v}_{\nu c}) \cdot \mathbf{k}} \left\{ \mathbf{k} \cdot \hat{\mathbf{p}}' - \frac{|\mathbf{p}'|}{E_{\mathbf{p}'}^2} [\mathbf{v}_{\nu c} \cdot \mathbf{k} - 4(\hat{\mathbf{p}}' \cdot \mathbf{v}_{\nu c})(\mathbf{k} \cdot \hat{\mathbf{p}}')] \right\}, \quad (2.16)$$

where we ignore terms of order  $\mathcal{O}(|\mathbf{v}_{\nu c}|^2)$ . While  $\mathbf{p}$  is defined in the DM halo frame, its counterpart  $\mathbf{p}'$  is in the CνF frame.

Notice that the denominator  $(\mathbf{p}' + E_{\mathbf{p}'} \mathbf{v}_{\nu c}) \cdot \mathbf{k}$  has a pole when  $\mathbf{p}' \cdot \mathbf{k} = -E_{\mathbf{p}'} \mathbf{v}_{\nu c} \cdot \mathbf{k}$ . It is this pole that generates the imaginary part of  $\delta\tilde{\rho}_\nu$ . With overdensity, the gravitational potential always has a limited size and cannot extend to infinity. Correspondingly, an imaginary part of the wavenumber,  $\mathbf{k} \rightarrow \mathbf{k} - i\epsilon$ , is introduced in the denominator for regularization [73]. Then, the Sokhotski-Plemelj-Weierstrass (SPW) theorem [94] can be used to extract the imaginary part,

$$\text{SPW theorem} \quad : \quad \lim_{\epsilon \rightarrow 0^+} \frac{1}{x - i\epsilon} = \mathcal{P} \left( \frac{1}{x} \right) + i\pi\delta(x), \quad (2.17)$$

with  $\mathcal{P}(1/x)$  indicating the principal value of the function  $1/x$ . It is clear that the imaginary part arises from the  $\delta$ -function and is non-zero if the angle between  $\mathbf{p}'$  and  $\mathbf{k}$  is  $\cos\theta \equiv \hat{\mathbf{p}}' \cdot \hat{\mathbf{k}} = -E_{\mathbf{p}'} \mathbf{v}_{\nu c} \cdot \hat{\mathbf{k}} / |\mathbf{p}'| \geq E_{\mathbf{p}'} |\mathbf{v}_{\nu c} \cdot \hat{\mathbf{k}}|$ . From Eq. (2.16), we obtain the imaginary part of the neutrino density fluctuations,

$$\text{Im}[\delta\tilde{\rho}_\nu] = - \frac{(\mathbf{v}_{\nu c} \cdot \hat{\mathbf{k}}) \tilde{\Psi}}{4\pi} \int d|\mathbf{p}'| (m_\nu^4 + 3m_\nu^2 |\mathbf{p}'|^2 + 2|\mathbf{p}'|^4) \frac{d\bar{f}_\nu}{d|\mathbf{p}'|} \Theta(|\mathbf{p}'| - E_{\mathbf{p}'} |\mathbf{v}_{\nu c} \cdot \hat{\mathbf{k}}|), \quad (2.18)$$

The derivation details can be found in App. B. Here, we use the on-shell condition  $E_{\mathbf{p}'}^2 = |\mathbf{p}'|^2 + m_\nu^2$ , and the Heaviside- $\Theta$  function to ensure that  $|\mathbf{p}'| \geq E_{\mathbf{p}'} |\mathbf{v}_{\nu c} \cdot \hat{\mathbf{k}}|$ . As we shall see in the next section, only the imaginary part of density fluctuations is relevant for the dipole galaxy correlation. Thus, calculating the corresponding real part is unnecessary. Eq. (2.18) explicitly shows that the non-zero relative velocity  $\mathbf{v}_{\nu c}$  leads to an imaginary part of neutrino energy density fluctuations in the Fourier space  $\delta\tilde{\rho}_\nu$ .

<sup>1</sup>For any function with dipole structure,  $A(-\mathbf{x}) = -A(\mathbf{x})$ , its Fourier transformation  $\tilde{A}(\mathbf{k}) \equiv \int d\mathbf{x} e^{-i\mathbf{k} \cdot \mathbf{x}} A(\mathbf{x})$  is a purely imaginary number since  $[\tilde{A}(\mathbf{k})]^* = \int d\mathbf{x} e^{i\mathbf{k} \cdot \mathbf{x}} A(\mathbf{x}) = \int d\mathbf{x} e^{-i\mathbf{k} \cdot \mathbf{x}} A(-\mathbf{x}) = -\int d\mathbf{x} e^{-i\mathbf{k} \cdot \mathbf{x}} A(\mathbf{x}) = -\tilde{A}(\mathbf{k})$ .

### 2.2.2. Matter Density Anisotropy Contributed by CνF

The fluctuations in the neutrino density contribute to the total matter density fluctuation that directly affects galaxy formation. Although cosmic neutrinos are usually treated as radiation, they can be both relativistic or non-relativistic in the late Universe depending on the mass eigenvalues. For heavy neutrinos that are already non-relativistic around redshift  $z = 10$ , they can be readily counted as matter. Although light neutrinos are still relativistic and hence should belong to radiation, its energy density is much smaller than the heavy neutrinos and hence it does not hurt to also count them as matter. For convenience, we define the sum of matter and neutrino densities as the total matter density and denote the corresponding overdensity as  $\tilde{\delta}_m$  in contrast to the genuine matter one  $\tilde{\delta}_{m0}$ .

Since the cosmic gravitational focusing leaves an imaginary correction in the neutrino density fluctuation, the total matter overdensity,  $\tilde{\delta}_m \equiv \delta\tilde{\rho}_m/\rho_m$ , is shifted from its real value,  $\tilde{\delta}_{m0}(\equiv \delta\rho_{m0}/\rho_m)$ , to a complex one,  $\tilde{\delta}_{m0} \rightarrow \tilde{\delta}_m \equiv \tilde{\delta}_{m0}(1 + i\tilde{\phi})$ . Here we have used  $\tilde{\phi}$  to parametrize the relative imaginary part while the magnitude is combined into  $\tilde{\delta}_{m0}$ . More concretely, the total matter overdensity is a sum of the matter overdensity  $\delta_{m0}$  and neutrino overdensities  $\delta_{\nu i}$ ,

$$\tilde{\delta}_m \equiv \tilde{\delta}_{m0}(1 + i\tilde{\phi}) = \tilde{\delta}_{m0} + \sum_{i=1}^3 \frac{\delta\tilde{\rho}_{\nu i}}{\rho_m} \equiv F_c\tilde{\delta}_c + F_\nu\tilde{\delta}_\nu, \quad (2.19)$$

where the first term is contributed mainly by DM while the second by CνF. Note that  $\tilde{\delta}_m$  is not simply a sum of the DM relative overdensity  $\tilde{\delta}_c$  and the neutrino one  $\tilde{\delta}_\nu$ . The weighting factors  $F_c$  and  $F_\nu$  [95] accounts for the fact that the total overdensity is defined as,  $\delta_m \equiv (\delta\rho_c + \delta\rho_\nu)/(\rho_c + \rho_\nu) \equiv F_c\delta_c + F_\nu\delta_\nu$  with  $F_c \equiv \rho_c/(\rho_c + \rho_\nu)$  and  $F_\nu \equiv \rho_\nu/(\rho_c + \rho_\nu)$ .

To obtain a neat form of  $\tilde{\phi}$ , we put Eq. (2.18) into Eq. (2.19) and replace the gravitational potential with the matter overdensity according to the Poisson equation,  $\tilde{\Psi} = -4\pi G a^2 \rho_m \tilde{\delta}_{m0}/|\mathbf{k}|^2$  [39]. The matter density  $\rho_m$  in  $\tilde{\Psi}$  cancels with the denominator in Eq. (2.19) and the overall factor  $\delta_{m0}$  is also factorized out,

$$\tilde{\phi} = \frac{G a^2}{|\mathbf{k}|^2} \sum_i (\mathbf{v}_{\nu ic} \cdot \hat{\mathbf{k}}) \int d|\mathbf{p}'| (m_i^4 + 3m_i^2|\mathbf{p}'|^2 + 2|\mathbf{p}'|^4) \frac{d\bar{f}_\nu}{d|\mathbf{p}'|} \Theta(|\mathbf{p}'| - E_{\mathbf{p}'}|\mathbf{v}_{\nu ic} \cdot \hat{\mathbf{k}}|), \quad (2.20)$$

where the phase space distribution  $\bar{f}_\nu(|\mathbf{p}'|) = 2/[e^{|\mathbf{p}'|/T} + 1]$  includes both the neutrino and anti-neutrino contributions. The  $1/|\mathbf{k}|^2$  dependence holds a clear physical significance. Below the neutrino free-streaming scale  $k_{\text{fs}}$ , the neutrino overdensity is suppressed by a factor  $(k_{\text{fs}}/|\mathbf{k}|)^2$  compared to the matter overdensity  $\delta_m$ . To extend beyond the static Boltzmann approximation, we can simply replace the factor  $(k_{\text{fs}}/|\mathbf{k}|)^2$  with  $(k_{\text{fs}}/|\mathbf{k}|)^2/(1 + k_{\text{fs}}/|\mathbf{k}|)^2$  [75]. This provides a more general formalism than our approach by incorporating a  $\Theta$  function in Eq. (C.4), with roughly the same result.

Since the square root of two neutrino mass differences,  $\sqrt{\Delta m_{21}^2} \approx 8.7 \times 10^{-3}$  eV and  $\sqrt{\Delta m_{31}^2} \approx 5 \times 10^{-2}$  eV measured by neutrino oscillation experiments [7], are much larger than

the current neutrino temperature,  $T_\nu \approx 1.7 \times 10^{-4}$  eV, at least one neutrino is non-relativistic for  $z \lesssim 10$ . In this approximation,  $|\mathbf{p}| \ll m_\nu$ , the second and third terms in the parenthesis of Eq. (2.20) can be ignored to give [73],

$$\tilde{\phi} \approx -\frac{2Ga^2}{|\mathbf{k}|^2} \sum_i \frac{m_i^4 (\mathbf{v}_{\nu_i c} \cdot \hat{\mathbf{k}})}{e^{m_i |\mathbf{v}_{\nu_i c} \cdot \hat{\mathbf{k}}|/T_\nu} + 1}. \quad (2.21)$$

To the leading order,  $\tilde{\phi}$  is proportional to the fourth power of neutrino mass,  $\sum m_i^4$ , which is the same as the drag force in Eq. (2.9). This is a prominent feature of the cosmic gravitational focusing and contrasts with the usual CMB and LSS constraints that are sensitive to the neutrino mass sum,  $\sum m_i$  [7]. Later, we show that their combination improves the sensitivity of cosmological constraints on the neutrino mass in Sec. 5.

Our result in Eq. (2.20) describes both relativistic and non-relativistic neutrinos. For relativistic neutrinos, we write Eq. (2.20) in terms of special functions with a variable change  $y \equiv |\mathbf{p}'|/T_\nu$ ,

$$\tilde{\phi} = \frac{Ga^2}{|\mathbf{k}|^2} \sum_i (\mathbf{v}_{\nu_i c} \cdot \hat{\mathbf{k}}) [m_i^4 f_0(y_i) + 3m_i^2 T_\nu^2 f_1(y_i) + 2T_\nu^4 f_2(y_i)], \quad (2.22)$$

where  $f_n(y_i) \equiv 2 \int_{y_i}^{\infty} dy y^{2n} d[e^y + 1]^{-1} / dy = - \int_{y_i}^{\infty} dy y^{2n} (1 + \cosh y)^{-1}$ . Note that the  $\Theta$ -function has been converted to  $y \geq y_i$  with  $y_i \equiv m_i |\mathbf{v}_{\nu_i c} \cdot \hat{\mathbf{k}}| T_\nu^{-1} [1 - (\mathbf{v}_{\nu_i c} \cdot \hat{\mathbf{k}})^2]^{-1/2}$  and implemented in the integration. The current bound on the neutrino mass sum is  $\sum m_i < 0.13$  eV at 95% C.L. [7, 68], which translates to  $m_\nu^{\text{lightest}} \lesssim 0.035$  eV for NO. Then, the heaviest neutrino mass is  $m_\nu^{\text{heaviest}} \lesssim 0.07$  eV and  $y_i \lesssim 0.5$ . The functions  $f_1(y_i)$  and  $f_2(y_i)$  can be safely approximated by their values at  $y_i = 0$ ,  $f_1(0) = -\pi^2/3$  and  $f_2(0) = -7\pi^4/15$ , with a precision of 0.7% since the next order is  $\mathcal{O}(y_i^3)$ . For  $f_0$ , the next order expansion,  $f_0(y_i) \approx -1 + y_i/2$ , is necessary to reach the 0.5% precision. Altogether, Eq. (2.22) is approximately,

$$\tilde{\phi} \approx -\frac{Ga^2}{|\mathbf{k}|^2} \sum_i (\mathbf{v}_{\nu_i c} \cdot \hat{\mathbf{k}}) \left[ m_i^4 \left( 1 - \frac{m_i |\mathbf{v}_{\nu_i c} \cdot \hat{\mathbf{k}}|}{2T_\nu} \right) + \pi^2 m_i^2 T_\nu^2 + \frac{14}{15} \pi^4 T_\nu^4 \right]. \quad (2.23)$$

Comparing with [73], the relativistic corrections  $m_i^2 T_\nu^2$  and  $T_\nu^4$  that are important for relativistic neutrinos are also taken into account. In addition, we keep the linear correction from  $m_i$  in the parenthesis whose effect can reach 25% for the heaviest neutrino. The overall minus sign is very important since it can determine whether the overdensity increases or decreases along the C $\nu$ F velocity.

In principle, the relativistic components should also include the CMB photon and the cosmic gravitational focusing can also happen between the CMB photons and DM halo. However, the massless photons can only contribute via the  $T_\gamma^4$  term which is negligibly smaller than the C $\nu$ F contribution. Even at redshift  $z = 10$ , the CMB temperature is around only  $10^{-3}$  eV which is at least one order smaller than  $\sqrt{\Delta m_{13}^2} \approx 5 \times 10^{-2}$  eV. With the fourth power, the CMB contribution is suppressed by at least four orders and can be safely omitted. A similar effect occurs between neutrino halos and the background photon to produce a dipole term in the CMB spectrum [69, 70].

### 2.2.3. Cosmic Gravitational Focusing with a Point Source

Although the classical picture with single particle trajectory provided in Sec. 2.2.1 can also handle the density perturbation using the Liouville's theorem [96], it is much more convenient to use the Boltzmann equation formalism which intrinsically handles overdensities. For easy comparison, we apply the Boltzmann formalism to a point source of gravitational potential.

Moving to the real space by Fourier transformation, the imaginary term of density fluctuation  $\delta\tilde{\rho}_m(\mathbf{k}) = \rho_m\tilde{\delta}_{m0}(1 + i\tilde{\phi})$  with  $\tilde{\phi}$  in Eq. (2.23) becomes,

$$\delta\rho_m(\mathbf{x}) \propto -i \int \frac{d^3\mathbf{k}}{(2\pi)^3} e^{i\mathbf{k}\cdot\mathbf{x}} \frac{1}{|\mathbf{k}|^2} \tilde{\delta}_{m0}(\mathbf{k})(\mathbf{v}_{\nu c} \cdot \hat{\mathbf{k}}). \quad (2.24)$$

For a point DM distribution at  $\mathbf{x}_i$ , i.e.,  $\delta_{m0}(\mathbf{x}) \propto \sum_i \delta_D^{(3)}(\mathbf{x} - \mathbf{x}_i)$  in the real space, the DM overdensity is plane wave,  $\tilde{\delta}_{m0}(\mathbf{k}) \propto \sum_i e^{-i\mathbf{k}\cdot\mathbf{x}_i}$ , in the Fourier space. Consequently, the Fourier transformation in Eq. (2.24) can be carried out analytically,

$$\delta\rho_m(\mathbf{x}) \propto -i \sum_i \int \frac{d|\mathbf{k}|}{(2\pi)^3} \int d\cos\theta e^{i|\mathbf{k}||\mathbf{x}-\mathbf{x}_i|\cos\theta} \int (\mathbf{v}_{\nu c} \cdot \hat{\mathbf{k}}) d\phi. \quad (2.25)$$

Choosing the relative position  $\mathbf{r}_i \equiv \mathbf{x} - \mathbf{x}_i$  as the  $z$  axis, the other two vectors  $\mathbf{k}$  and  $\mathbf{v}_{\nu c}$  can be parameterized as,  $\hat{\mathbf{k}} \equiv (\sin\theta \cos\phi, \sin\theta \sin\phi, \cos\theta)$  and  $\hat{\mathbf{v}}_{\nu c} \equiv (\sin\theta_v \cos\phi_v, \sin\theta_v \sin\phi_v, \cos\theta_v)$ . After integration, the  $(x, y)$  components vanish since  $\int (\cos\phi, \sin\phi) d\phi = 0$  and only the third component  $\sim \cos\theta \cos\theta_v$  survives. Then, we can directly integrate out the zenith angle  $\cos\theta$ ,

$$\delta\rho_m(\mathbf{x}) \propto 2 \sum_i (\mathbf{v}_{\nu c} \cdot \mathbf{r}_i) \int \frac{d|\mathbf{k}|}{(2\pi)^2} \frac{J_1(|\mathbf{k}||\mathbf{r}_i|)}{|\mathbf{r}_i|}, \quad (2.26)$$

where  $J_1(x) \equiv \sin x/x^2 - \cos x/x$ , is the first spherical Bessel function. We see that the  $-i$  factor is absorbed into the  $d\cos\theta$  integration to give a real number. The minus sign in Eq. (2.23) is to ensure that C $\nu$ F focuses downstream. The prefactor  $\hat{\mathbf{v}} \cdot \hat{\mathbf{r}}$  indicates that the density increases along the direction of  $\mathbf{v}_{\nu c}$ .

## 3. Galaxy Correlation with Cosmic Gravitational Focusing

Since both neutrinos and DM are invisible, their cosmic gravitational focusing and the resultant density fluctuations cannot be observed directly. Contributing to the matter density fluctuation, C $\nu$ F can affect galaxy distribution. So the galaxy correlation functions can be used to trace the cosmic gravitational focusing. In particular, the C $\nu$ F focusing effect can manifest itself in the galaxy dipole correlation function as imaginary power spectrum in the Fourier space [72, 73] as well as the galaxy weak lensing [71]. We derive the imaginary power spectrum with the redshift-space distortion (RSD) in Sec. 3.1 to show its dependence on the neutrino masses. The signal-to-noise ratio (SNR) for observation is summarized in Sec. 3.2.

### 3.1. Imaginary Galaxy Power Spectrum with RSD

In the late Universe ( $z \lesssim 100$ ), the baryon matter tightly follows the density fluctuations contributed by mainly DM but also the CνF to form galaxies. Consequently, the galaxy distribution encodes the information of the cold DM ( $\delta_c$ ) and CνF ( $\delta_\nu$ ) overdensities. To be more exact, the galaxy overdensity is a linear function of the DM and CνF overdensities with different bias [95],

$$\delta_{g\alpha} = b_c^\alpha F_c \delta_c + b_\nu^\alpha F_\nu \delta_\nu \quad \Rightarrow \quad \tilde{\delta}_{g\alpha} \approx \tilde{\delta}_{m0} \left( b_c^\alpha + i b_\nu^\alpha \tilde{\phi} \right). \quad (3.1)$$

In the approximation, we have used the fact that the real part is mainly contributed by DM,  $\text{Re}[\delta_{g\alpha}] \approx b_c^\alpha \delta_{m0}$ , while the imaginary one comes from CνF,  $\text{Im}[\delta_{g\alpha}] = b_\nu^\alpha \text{Im}[F_\nu \delta_\nu] = i b_\nu^\alpha \delta_{m0} \tilde{\phi}$ . As defined in Eq. (2.19), the total matter density is  $\tilde{\delta}_m \equiv \tilde{\delta}_{m0}(1 + i\tilde{\phi})$  which implies that  $F_c \tilde{\delta}_c = \tilde{\delta}_{m0}$  and  $F_\nu \tilde{\delta}_\nu = i \delta_{m0} \tilde{\phi}$ . Note that  $F_\nu \tilde{\delta}_\nu$  here is essentially its imaginary part while its real part can be neglected or already combined into  $F_c \tilde{\delta}_c$ .

The observed galaxy overdensity in the redshift space ( $\delta_{g\alpha, \text{RSD}}$ ) is different from the one in the real space ( $\delta_{g\alpha}$ ) due to the Doppler shift caused by the galaxy peculiar velocity  $\mathbf{u}_m$ . This effect is known as the RSD [39],

$$\delta_{g\alpha, \text{RSD}}(\mathbf{x}) \equiv \delta_{g\alpha}(\mathbf{x}) - \frac{\partial}{\partial x} \left( \frac{\mathbf{u}_m \cdot \hat{\mathbf{x}}}{aH} \right). \quad (3.2)$$

For a specific Fourier mode with wavenumber  $\mathbf{k}$ , the spatial derivative  $\partial/\partial x \equiv \hat{\mathbf{x}} \cdot \nabla_{\mathbf{x}}$  becomes  $\hat{\mathbf{x}} \cdot i\mathbf{k}$ . Since the curl part damps out during the cosmic evolution [97], the peculiar velocity can be reparameterized,  $\tilde{\mathbf{u}}_m = -i\tilde{\theta}_m \mathbf{k}/|\mathbf{k}|^2$ , in terms of the velocity divergence  $\tilde{\theta}_m$  which can be further expressed in terms of  $\tilde{\delta}_m$  according to the linear Boltzmann equation,  $a\dot{\tilde{\delta}}_m + \tilde{\theta}_m \approx 0$ . Altogether, the overdensity with RSD becomes,  $\tilde{\delta}_{g\alpha, \text{RSD}} = \tilde{\delta}_{g\alpha} + \mu_{\mathbf{k}}^2 \tilde{\delta}_m / H$  where  $\mu_{\mathbf{k}} \equiv \hat{\mathbf{x}} \cdot \hat{\mathbf{k}}$ . Together with the  $\tilde{\delta}_{g\alpha}$  in Eq. (3.1) and the matter overdensity  $\tilde{\delta}_m$  elaborated in Sec. 2.2.2,  $\tilde{\delta}_{g\alpha, \text{RSD}}$  becomes,

$$\tilde{\delta}_{g\alpha, \text{RSD}} = b_c^\alpha \tilde{\delta}_{m0} + \frac{\mu_{\mathbf{k}}^2}{H} \dot{\tilde{\delta}}_{m0} + i \left[ b_\nu^\alpha \tilde{\delta}_{m0} \tilde{\phi} + \frac{\mu_{\mathbf{k}}^2}{H} \left( \dot{\tilde{\delta}}_{m0} \tilde{\phi} + \tilde{\delta}_{m0} \dot{\tilde{\phi}} \right) \right]. \quad (3.3)$$

For convenience, we have disentangled the real and imaginary parts.

The observable in galaxy survey is the galaxy two-point cross correlation functions,  $\mathcal{P}_{\alpha\beta} \equiv \tilde{\delta}_{g\alpha, \text{RSD}} \tilde{\delta}_{g\beta, \text{RSD}}^*$ , whose imaginary part is non-zero only if  $\tilde{\phi} \neq 0$ . For generality, we use  $\alpha$  and  $\beta$  to indicate different galaxy categories for cross correlation. The imaginary part of the galaxy cross correlation is,

$$\text{Im}[\mathcal{P}_{\alpha\beta}] = - (b_c^\alpha b_\nu^\beta - b_\nu^\alpha b_c^\beta) \tilde{\delta}_{m0}^2 \tilde{\phi} - (b_c^\alpha - b_c^\beta) \frac{\mu_{\mathbf{k}}^2}{H} \tilde{\delta}_{m0} (\dot{\tilde{\delta}}_{m0} \tilde{\phi} + \tilde{\delta}_{m0} \dot{\tilde{\phi}}) + (b_\nu^\alpha - b_\nu^\beta) \frac{\mu_{\mathbf{k}}^2}{H} \dot{\tilde{\delta}}_{m0} \tilde{\delta}_{m0} \tilde{\phi}. \quad (3.4)$$

with general bias  $b_c$  and  $b_\nu$  for DM and CνF components, respectively. The values of these bias parameters are up to choice. For example, Ref. [72] takes  $b_\nu^\alpha = b_\nu^\beta = 1$  but does not consider the RSD correction while Ref. [73] considers the RSD correction but assumes  $b_\nu^{\alpha, \beta} = b_c^{\alpha, \beta}$ .

Notice that the observable in Eq. (3.4) is zero if both  $b_c^\alpha = b_c^\beta$  and  $b_\nu^\alpha = b_\nu^\beta$ . In other words, the cosmic gravitational focusing can be measured only via the cross correlation of two galaxy categories that have at least one different bias. The neutrino bias is close to 1 up to  $\lesssim 2\%$  corrections [95]. For simplicity, we take  $b_\nu^\alpha = b_\nu^\beta = 1$ . Eq. (3.4) can be further simplified by using  $\tilde{\delta}_{m0} = Hf\tilde{\delta}_{m0}$ ,

$$\text{Im}[\tilde{\delta}_{g\alpha,\text{RSD}}\tilde{\delta}_{g\beta,\text{RSD}}^*] = -i\Delta b \left[ \mu_k^2 \frac{\tilde{\phi}}{H} + (f\mu_k^2 + 1)\tilde{\phi} \right] \tilde{\delta}_{m0}^2, \quad (3.5)$$

where  $\Delta b \equiv b_c^\alpha - b_c^\beta$  and  $f \equiv d \ln D_+ / d \ln a \approx \Omega_m(z)^\gamma$  with  $\gamma \approx 0.55$  [76]. Assuming  $b_\nu^{\alpha,\beta} = b_c^{\alpha,\beta}$ , all those  $\tilde{\phi}$  terms in Eq. (3.4) vanishes and only the first term of Eq. (3.5) can survive [73]. Our result has the additional second term with  $b_\nu^\alpha \neq b_c^\alpha$  which is more reasonable since C $\nu$ F and DM should have different bias with different clustering properties [95]. Since the two terms add up with a positive sign in between, the different bias between neutrino and DM would amplify the cross correlation. This would make the cosmic gravitational focusing more sensitive to the neutrino masses.

### 3.2. The Signal-to-Noise Ratio of Galaxy Cross-Correlation

The cosmic gravitational focusing signal is defined as the imaginary part of the galaxy cross-correlation [73] as shown in Eq. (3.5),  $\mathcal{S} \equiv \text{Im}[\tilde{\delta}_{g\alpha,\text{RSD}}\tilde{\delta}_{g\beta,\text{RSD}}^*]$ . However, a typical cosmological observation is subject to two sources of statistical uncertainties: (1) The random fluctuations of the observable (in our case the galaxy overdensity  $\delta_g$ ) and (2) A Poisson white noise ( $\epsilon$ ). In the presence of a Poisson noise, the observed signal is shifted from the true observable,  $\tilde{\delta}_{g\alpha} \rightarrow \tilde{\delta}'_{g\alpha} \equiv \tilde{\delta}_{g\alpha} + \epsilon_\alpha$  [39]. Since  $\delta_{g\alpha}$  and  $\epsilon_\alpha$  are independent, any dependence on  $\epsilon_\alpha$  averages out for both linear and quadratic terms with  $\alpha \neq \beta$ . Then the ensemble average of  $\mathcal{S} \equiv \text{Im}[\tilde{\delta}'_{g\alpha,\text{RSD}}\tilde{\delta}'_{g\beta,\text{RSD}}^*]$  in the presence of white noise,

$$\langle \mathcal{S} \rangle \equiv \text{Im}[\langle \tilde{\delta}'_{g\alpha,\text{RSD}}\tilde{\delta}'_{g\beta,\text{RSD}}^* \rangle] = \text{Im}[\langle \tilde{\delta}_{g\alpha,\text{RSD}}\tilde{\delta}_{g\beta,\text{RSD}}^* \rangle] = \text{Im}[P_{\alpha\beta}], \quad (3.6)$$

reduces back to the original imaginary parts of the galaxy power spectrum,  $P_{\alpha\beta} \equiv \langle \tilde{\delta}_{g\alpha,\text{RSD}}\tilde{\delta}_{g\beta,\text{RSD}}^* \rangle$ . In other words, the influence of white noises  $\epsilon_\alpha$  diminishes in the cross correlation signal.

The noise/uncertainty of the measurement can be estimated as the variance of the signal  $\mathcal{N}^2 \equiv \langle (\mathcal{S} - \langle \mathcal{S} \rangle)^2 \rangle$  [98]. More concretely, it can be written as the determinant of the covariance matrix  $C_{\alpha\beta}$  in terms of the galaxy power spectrum and comoving number densities  $n_\alpha (\equiv \langle \epsilon_\alpha \epsilon_\alpha^* \rangle^{-1})$  [98],

$$\mathcal{N}^2 = \frac{1}{2} \text{Det}[C] + 2 \text{Im}^2[P_{\alpha\beta}] \approx \frac{1}{2} \text{Det}[C] \quad \text{with} \quad C_{\alpha\beta} \equiv \begin{pmatrix} P_{\alpha\alpha} + n_\alpha^{-1} & P_{\alpha\beta} \\ P_{\beta\alpha} & P_{\beta\beta} + n_\beta^{-1} \end{pmatrix}. \quad (3.7)$$

Since  $\text{Im}[P_{\alpha\beta}] \ll \text{Det}[C]$ , the error may be safely approximated using the half determinant,  $\mathcal{N}^2 \approx \text{Det}[C]/2$  [73, 98].

We construct the log-likelihood  $\langle \mathcal{S} \rangle^2 / \mathcal{N}^2$  from the SNR using Eq. (3.5) and Eq. (3.7). The total sensitivity is obtained by integrating over the wave number  $\mathbf{k}$  and summing up the redshift  $z_i$  bins,

$$-2 \ln L = \sum_{z_i, \nu_j} V_i \int \frac{d^3 \mathbf{k}}{(2\pi)^3} \frac{2\Delta b}{\text{Det}[\mathbf{C}]} \left\langle \left[ \mu_{\mathbf{k}}^2 \frac{\dot{\tilde{\phi}}_{\nu_j}}{H} + (f\mu_{\mathbf{k}}^2 + 1)\tilde{\phi}_{\nu_j} \right] \tilde{\delta}_{m0}^2 \right\rangle^2, \quad (3.8)$$

where  $V_i$  is the volume for the  $z_i$  redshift bin.

Since  $\tilde{\phi} \propto \mathbf{v}_{\nu c} = \mathbf{v}_{\nu c}^{\text{bg}} + \mathbf{u}_{\nu c}$  which is a linear combination of the background velocity  $\mathbf{v}_{\nu c}^{\text{bg}}$  and the relative velocity fluctuation  $\mathbf{u}_{\nu c}$ , then  $\langle \tilde{\phi} \tilde{\delta}_{m0}^2 \rangle \propto \mathbf{v}_{\nu c}^{\text{bg}} \langle \tilde{\delta}_{m0}^2 \rangle + \langle \mathbf{u}_{\nu c} \tilde{\delta}_{m0}^2 \rangle$  with  $\langle \mathbf{u}_{\nu c} \rangle = 0$ . The second term is a third power of random Gaussian variables and is zero. To calculate  $\mathbf{v}_{\nu c}^{\text{bg}}$ , we make the approximation  $\mathbf{v}_{\nu c}^{\text{bg}} = \sqrt{\langle \mathbf{v}_{\nu c}^2 \rangle} + \mathcal{O}(\mathbf{u}_{\nu c}^2)$  [72, 73, 99, 100], thus  $\langle \tilde{\phi} \tilde{\delta}_{m0}^2 \rangle \propto \sqrt{\langle \mathbf{v}_{\nu c}^2 \rangle} \langle \tilde{\delta}_{m0}^2 \rangle$ . In other words,  $\langle \tilde{\phi} \tilde{\delta}_{m0}^2 \rangle \approx \sqrt{\langle \tilde{\phi}^2 \rangle} P_{m0}$ , where  $P_{m0} \equiv \langle \delta_{m0}^2 \rangle$  is the matter power spectrum seeded in the early Universe. Similar arguments can also apply for  $\dot{\tilde{\phi}}$ . The ensemble average of  $\tilde{\phi}^2$  does not depend on the direction of the wave number  $\mathbf{k}$  and the integration over  $d\Omega_{\mathbf{k}}$  in Eq. (3.8) can be performed explicitly,

$$-2 \ln L = \sum_{z_i, \nu_j} \frac{\Delta b^2 V_i}{5\pi^2} \int d \ln |\mathbf{k}| \frac{|\mathbf{k}|^3 P_{m0}^2}{\text{Det}[\mathbf{C}]} \left\{ \left[ \frac{\sqrt{\langle \dot{\tilde{\phi}}_i^2 \rangle}}{H} + \left( f + \frac{5}{3} \right) \sqrt{\langle \tilde{\phi}^2 \rangle} \right]^2 + \frac{20}{9} \langle \tilde{\phi}^2 \rangle \right\}. \quad (3.9)$$

Notice that the terms containing  $\langle \tilde{\phi}^2 \rangle$  in Eq. (3.9) are extensions of the results in [73], especially the Eq.(A13) therein. Both  $\langle \tilde{\phi}^2 \rangle$  terms are extra positive contributions. The ensemble average values  $\langle \dot{\tilde{\phi}}_i^2 \rangle$  and  $\langle \tilde{\phi}^2 \rangle$  can be found in App. C. These averages are proportional to  $\langle \mathbf{v}_{\nu c}^2 \rangle$ , which decreases at large scale according to the N-body simulation [101]. We add a  $\Theta$  function [73] inside the velocity integration to capture this feature, as explicitly shown in Eq. (C.4).

The imaginary contribution to the cross power spectrum in Eq. (3.8) can be understood as a manifestation of the squeezed-limit bispectrum. When  $|\mathbf{k}_1| \approx 0$ , the average  $\langle v(\mathbf{k}_1) \delta_m(\mathbf{k}) \delta_m(\mathbf{k}') \rangle$  can be approximated as  $v \langle \delta_m^2 \rangle$ , where the coefficient  $v$  is the response of the cross power spectrum to the presence of a long-wavelength relative velocity field. This procedure is similar to the squeezed limits of the nonlinear matter power spectrum in the presence of a long-wavelength density field [102–104]. In reality, the two-point functions, viewed as squeezed limit of the three-point functions, encapsulate the same information of the gravitational focusing effect as the latter.

## 4. Galaxy Number Density and Bias at DESI

The Dark Energy Spectroscopic Instrument (DESI) [76, 77] is a ground-based experiment to collect around 40 million galaxies and quasars in 5 years by covering 14,000 square degree of



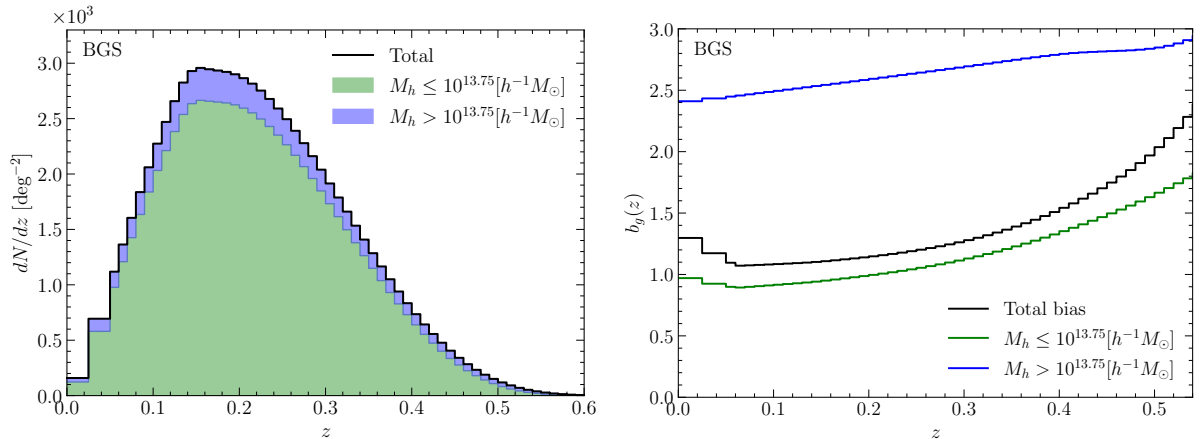


Fig. 1: The observable galaxy number distribution (Left) and bias (Right) for the BGS category by using the lightcone catalogue [105, 106]. The two sub-categories are divided according to the halo mass  $M_h < 10^{13.75} h^{-1} M_\odot$  (green) and  $M_h > 10^{13.75} h^{-1} M_\odot$  (blue). For comparison, the combined values are shown as black lines in both panels.

the sky. The DESI instrument, the Mayall Telescope at the Kitt Peak National Observatory, is capable of detecting light from extragalactic sources in the three optical bands ( $r$ ,  $g$ , and  $b$ ) with wave length from 360 nm to 980 nm. The DESI survey is expected to detect around 10 million bright galaxies for low redshift ( $z < 0.6$ ) and 30 million faint galaxies and quasars at intermediate redshift ( $0.6 < z < 2$ ). The observation and characterization capabilities of the DESI experiments are perfect for detecting the cosmic gravitational focusing effect. So we take DESI for illustration. More specifically, we use halo occupation distribution (HOD) based on the lightcone catalogue [105, 106] to determine the BGS number density in Sec. 4.1 and bias in Sec. 4.2. Finally, the faint galaxies are summarized in Sec. 4.3.

#### 4.1. BGS Number Density

As pointed out above Eq. (3.5) that the cosmic gravitational focusing appears in the cross correlation function of different galaxy categories. The DESI instrument can make spectroscopic observations of four distinct categories of extragalactic sources [76]: the bright galaxy sample (BGS) at  $0.05 < z < 0.4$ , luminous red galaxies (LRGs) at  $0.4 < z < 1.0$ , star-forming emission line galaxies (ELG) at  $0.6 < z < 1.6$ , and quasi-stellar objects (QSO) at  $z > 0.6$ . In the low redshift region  $z < 0.4$ , BGS has the largest population. To maximize the SNR, we split the BGS category into two and consider the internal cross correlation. The remaining LRG, ELG, and QSO can also contribute with three cross correlations among them to be discussed in Sec. 4.3.

The galaxy formation is mainly determined by the halo distribution, namely, the halo mass function (HMF)  $dn/d\ln M_h$  that describes the halo number density  $n$  as a function of the halo mass  $M_h$  [39, 107, 108]. Given a halo mass  $M_h$ , the HOD gives the average number  $\langle N(M_h) \rangle$  of

galaxies [109]. Then their convolution gives the galaxy number density,

$$n_g(z) \equiv \int d \ln M_h \frac{dn(z)}{d \ln M_h} \langle N(M_h) \rangle. \quad (4.1)$$

The redshift dependence comes from the HMF  $dn(z)/d \ln M_h$  which can be calculated by the `halomod` package [110, 111] with the SMT model configuration [112] and the cosmological parameters given by Planck 2018 [67]. The HOD is calculated by `hodpy` [105, 106] which uses a Gaussian empirical parametrization of  $\langle N(M_h) \rangle$  [113] to fit the Schechter luminosity function [114] obtained from the GAMMA [115] and SDSS [116] data (for a more detailed description of the method see [105]). Since only those halos with mass above a typical threshold value  $M_{\min} = 10^{11} h^{-1} M_\odot$  can host galaxies, the HOD  $\langle N(M_h) \rangle$  goes to zero for  $M_h < M_{\min}$ . On the other hand, the heavy halo abundance is exponentially suppressed. Above  $M_{\max} = 10^{16} h^{-1} M_\odot$  there is almost no halo which can be imposed by requiring  $M_h < M_{\max}$ .

Finally, the total number of galaxies,  $d^2 N/dz d\Omega$ , is obtained by multiplying galaxy number density  $n_g$  by the comoving volume per redshift and square degree  $d^2 V/dz d\Omega = [\int dz'/H(z')]^2 (\pi/180)^2 [\Delta z/H(z)]$ . The left panel of Fig. 1 shows the BGS distributions per square degree for the two sub-categories,  $M_h < 10^{13.75} h^{-1} M_\odot$  (green) and  $M_h > 10^{13.75} h^{-1} M_\odot$  (blue). Dividing galaxies into sub-categories according to the halo mass [117] is adopted to differentiate the halo bias as elaborated below in Sec. 4.2. The total height of the two regions shows the total number of observable galaxies for the BGS category. Since the number density  $n_g$  decreases while the volume increases with the redshift  $z$ ,  $\propto (1+z)^3$ , the galaxies number per square degree first increases to reach its maximum at  $z \approx 0.15$  and then decreases fast. In other words, the most sensitivity contributed by the BGS category should come from  $z \in (0.1 \sim 0.3)$ .

## 4.2. BGS Bias

The galaxy bias is obtained by integrating over the same distribution in Eq. (4.1) but with the halo bias  $b_h(M_h, z)$  [109] as an extra weight,

$$b_g(z) \equiv \frac{1}{n_g} \int d \ln M_h \frac{dn(z)}{d \ln M_h} \langle N(M_h) \rangle b_h(M_h, z). \quad (4.2)$$

In addition to the HMF, the redshift dependence also comes from the halo bias function  $b_h(M_h, z)$  for which we use the ST99 [118] configuration in the `halomod` package [110, 111].

As emphasized above, the cosmic gravitational focusing signal in Eq. (3.5) requires the separation of galaxies into two categories with different bias. This can be realized by dividing the BGS category into two sub-categories according to the halo mass,  $M_h < M_{\text{split}}$  and  $M_h > M_{\text{split}}$  [117]. For an observation, the halo mass can be related to its galaxy luminosity [119] with a cluster finder algorithm [120, 121] to reach a precision of  $\Delta \log_{10} M_h/M_\odot h^{-1} \sim 0.4$  [122]. Accordingly, the number densities  $n_1$  ( $n_2$ ) in Eq. (4.1) are obtained by integrating the halo mass  $M_h$  over the two mass ranges,  $M_{\min} < M_h < M_{\text{split}}$  and  $M_{\text{split}} < M_h < M_{\max}$ , respectively.

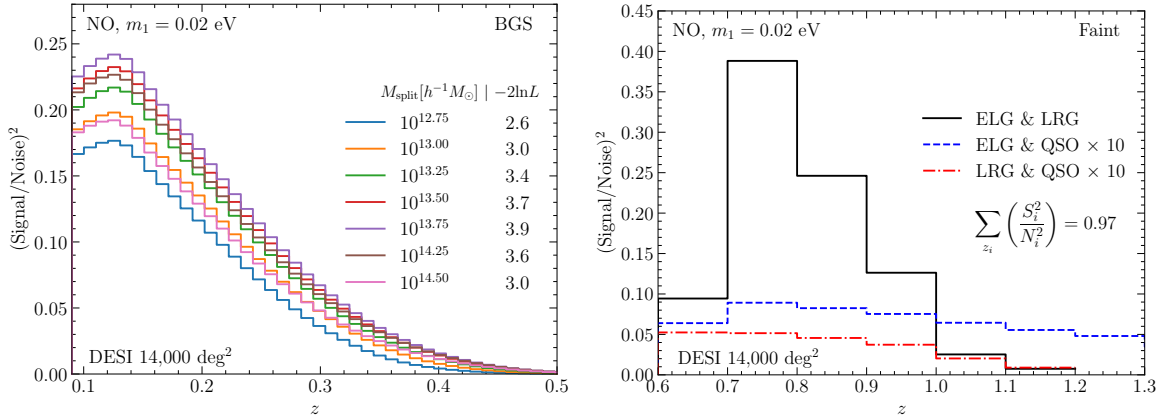


Fig. 2: The SNR of cosmic gravitational focusing for the BGS (Left) and remaining (Right) catalogues with the lightest neutrino mass  $m_1 = 0.02$  eV and the NO. While the BGS survey is mainly at the low redshift region  $z < 0.6$ , the faint galaxy (LRG, ELG, and QSO) surveys reside at higher redshift  $z > 0.6$ . A total area of 14,000 square degree can be observed at the DESI instrument.

The SNR in Eq. (3.9) is proportional to the bias difference of two galaxies  $\Delta b \equiv b_1 - b_2$ . On the other hand, the shot noise decreases with  $n_1$  and  $n_2$  in the determinant of the covariance matrix according to Eq. (3.7). Hence, the sensitivity increases with both bias difference  $\Delta b$  and galaxy numbers  $n_i$ . As we have seen above, the mass splitting parameter  $M_{\text{split}}$  affects both  $n_i$  and  $\Delta b$  via integration limits. Namely, if  $M_{\text{split}}$  increases,  $\Delta b$  and  $n_1$  increases while  $n_2$  decreases, and vice versa. Although larger  $\Delta b$  and  $n_1$  can increase the sensitivity, the decrease of  $n_2$  will make it worse. The optimal value of  $M_{\text{split}}$  can be found by maximizing the SNR. Our result is shown in the left panel of Fig. 2 for NO and  $m_1 = 0.02$  eV. Several typical values in the range of  $M_{\text{split}} \in [10^{12.75}, 10^{14.5}] h^{-1} M_{\odot}$  are shown for comparison. The total log-likelihood starts from 2.6 with  $M_{\text{split}} = 10^{12.75} h^{-1} M_{\odot}$  and increases to its maximal value 3.9 with  $M_{\text{split}} = 10^{13.75} h^{-1} M_{\odot}$ . So we take  $M_{\text{split}} = 10^{13.75} h^{-1} M_{\odot}$  as a benchmark point for our results in Fig. 1 and later discussions.

The right panel of Fig. 1 shows the galaxy bias of the BGS category. For the whole BGS category, a major feature of the black line is that the BGS bias increases with redshift. This is because a flux-limited sample at high redshift is intrinsically brighter and hence has a larger halo mass which usually leads to more galaxies. The green and blue lines denote the two sub-categories of the BGS:  $M_h < 10^{13.75} h^{-1} M_{\odot}$  and  $M_h > 10^{13.75} h^{-1} M_{\odot}$ . The heavier sub-categories in blue easily host more galaxies and therefore have a larger bias  $b_g > 2.4$  than the lighter sub-category one  $2 > b_g > 1$ . The bias difference between the two sub-categories approaches to  $\Delta b \approx 1$  which is quite sizable.

Fig. 3 shows the scales that contribute the most to the SNR with three typical redshift values  $z = (0.1, 0.2, \text{ and } 0.3)$  for the BGS sub-categories. What we plot is the integrand in Eq. (3.9) which is a function of the wave number  $\mathbf{k}$  and proportional to  $|\mathbf{k}|^3 P_m^2(\mathbf{k}) \tilde{\phi}^2$ . With higher redshift, the contribution to SNR is smaller since the matter clustering is smaller at

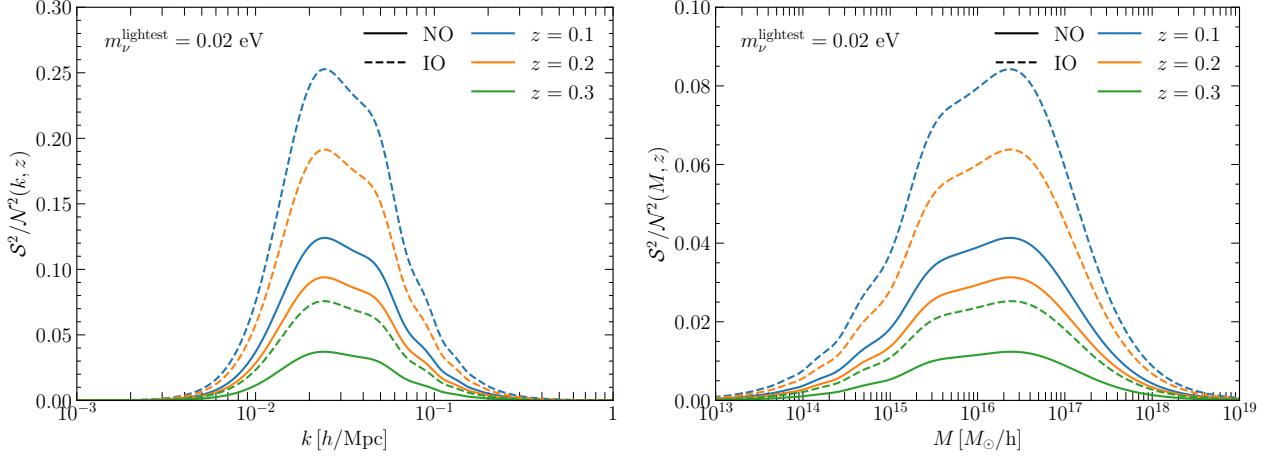


Fig. 3: The SNR integrand for both NO and IO with the lightest neutrino mass  $m_{\nu}^{\text{lightest}} = 0.02$  eV at redshifts  $z = 0.1, 0.2,$  and  $0.3$ . The left panel shows the SNR integrand as a function of the comoving wave number  $|\mathbf{k}|$  while the right panel takes the mass enclosed in the corresponding radius  $R \equiv 1/|\mathbf{k}|$ .

earlier stages. Between NO and IO, the latter has larger effect with two heavy neutrinos. At large scales (small  $|\mathbf{k}|$ ), the integration kernel  $|\mathbf{k}|^3 P_m^2(\mathbf{k}) \tilde{\phi}^2 \propto |\mathbf{k}|^3$  (with matter power spectrum  $P_m(\mathbf{k}) \sim |\mathbf{k}|$  [39] and  $\tilde{\phi} \propto |\mathbf{v}|/|\mathbf{k}|^2 \propto 1/|\mathbf{k}|$  in Eq. (2.22) since the velocity  $\mathbf{v} \propto \nabla \Psi \propto |\mathbf{k}|$ ) shown in Fig. 3 is suppressed by small  $\mathbf{k}$ . Also, the peak shifts from the  $0.01 h/\text{Mpc}$  for the power spectrum to  $0.02 h/\text{Mpc}$ . The largest contribution to the SNR values occurs in the region of  $10^{-2} h/\text{Mpc} < k < 10^{-1} h/\text{Mpc}$  which corresponds to the length scales of  $(15 \sim 150)$  Mpc with the dimensionless Hubble rate  $h = 0.67$ . This range is inside the region where the linear bias choice in Eq. (3.1) applies [123]. Such linear bias does not suffer much from the uncertainty at small scales comparing with the usual mass sum constraint based on the small scale suppression. The decreasing on the large- $k$  end comes from the matter power spectrum  $|\mathbf{k}|^3 P_m^2(\mathbf{k}) \tilde{\phi}^2 \sim 1/|\mathbf{k}|^5$  with  $P_m(\mathbf{k}) \sim 1/|\mathbf{k}|^3$  [39].

The integration over  $|\mathbf{k}|$  in Eq. (3.9) can be rewritten,  $-2 \ln L \equiv \sum_{z, \nu_i} \int \mathcal{S}^2/\mathcal{N}^2(|\mathbf{k}|, z) d \ln |\mathbf{k}| \equiv \sum_{z, \nu_i} \int \mathcal{S}^2/\mathcal{N}^2(M, z) d \ln M$ , in terms of the corresponding mass  $M(R) \equiv \rho_m 4\pi R^3/3$  enclosed in the sphere with radius  $R \equiv 1/|\mathbf{k}|$ . Correspondingly, the integration interval changes as  $dM = -\rho_m 4\pi d|\mathbf{k}|/|\mathbf{k}|^4 = -3M d|\mathbf{k}|/|\mathbf{k}|$  and consequently  $d \ln M = -3 d \ln |\mathbf{k}|$ . For large mass (small  $|\mathbf{k}|$ ), the  $\mathcal{S}^2/\mathcal{N}^2(M, z) \propto 1/M$  while for small mass (large  $|\mathbf{k}|$ ), the  $\mathcal{S}^2/\mathcal{N}^2(M, z) \propto M^{5/3}$  as shown in the right panel of Fig. 3. With the critical density  $\rho_{\text{cr}} = 2.7 \times 10^{11} h^2 M_{\odot}/\text{Mpc}^3$  and matter fraction  $\Omega_m \approx 0.3$ , the corresponding mass region enclosed in the sphere with radius  $R = 1/|\mathbf{k}|$  ranges from  $10^{14} M_{\odot}/h$  to  $10^{18} M_{\odot}/h$ . The peak radius  $\sim 75$  Mpc ( $|\mathbf{k}| \approx 0.02 h/\text{Mpc}$ ) in the left panel corresponds to the peak mass  $\sim 10^{16} M_{\odot}/h$  in the right panel. Since such a volume can accommodate a few hundreds of halos with typical halo size of a few Mpc [39], the corresponding halo mass is consistent with our mass splitting point  $M_{\text{split}} \times 100 \approx 10^{16} M_{\odot}/h$ . Between the two neutrino mass orderings, IO (solid) has almost two times larger SNR than NO (dashed) in both panels since the former has two nearly degenerate heavy neutrinos while later has only one.

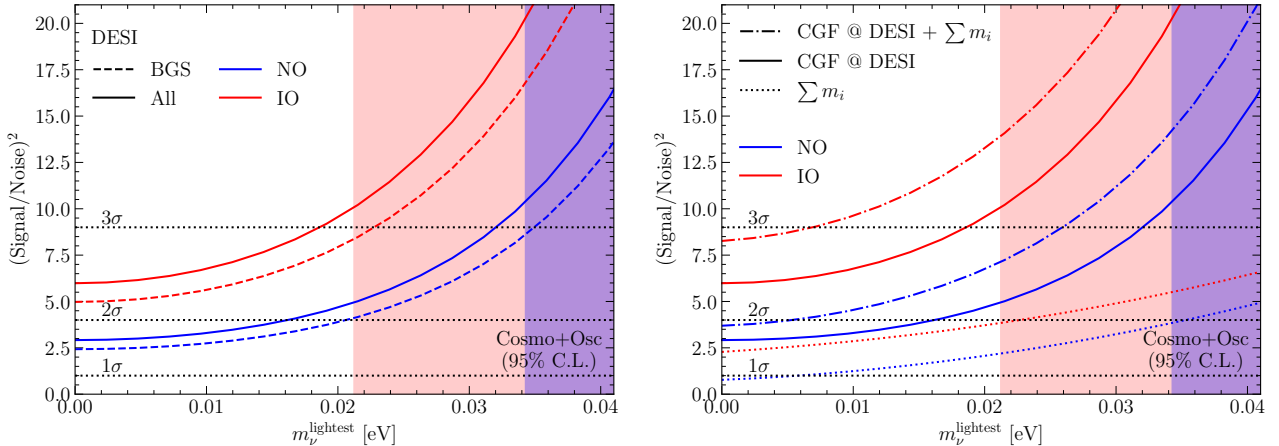


Fig. 4: (Left) The SNR at DESI for both NO (blue) and IO (red) cases as function of the lightest neutrino mass ( $m_\nu^{\text{lightest}}$ ) with BGS alone (dashed) or all categories (solid). (Right) The comparison of cosmic gravitational focusing sensitivity at DESI (CGF @ DESI, solid) with the existing cosmological constraints (dotted). Their synergy is also plotted as dot-dashed line. For both panels, the shaded regions indicate the current constraints ( $\sum m_i < 0.13$  eV at 95% C.L.) from cosmology and neutrino oscillation experiments for both NO (blue) and IO (red).

### 4.3. Faint Galaxies

For the faint galaxy population at higher redshift ( $z > 0.6$ ), including LRG, ELG, and QSO, we use the number density distributions and biases summarized in the DESI paper [76, 77], such as the Table 2.3 of [76]. The galaxy bias is taken as  $b_{\text{LRG}}(z)D(z) = 1.7$  (LRG) [76],  $b_{\text{ELG}}(z)D(z) = 0.84$  (ELG) [124], and  $b_{\text{QSO}}(z)D(z) = 1.2$  (QSO) [125], respectively. With dependence on the linear growth factor  $D(z)$ , the galaxy bias is also a function of redshift. In the right panel of Fig. 2, we show the SNR for all the three possible correlations among the faint galaxy categories. The total SNR is roughly 0.97 which is smaller than the BGS. Among them, the correlation between ELG and LRG dominates which is a direct consequence of the fact that the observable QSO population is much smaller than ELG and LRG.

## 5. DESI Sensitivity and Synergy with Mass Sum Constraints

With the knowledge of galaxy distributions and bias, we can estimate the DESI sensitivity on the lightest neutrino mass. As already implemented in Fig. 2, the DESI instrument can observe 14,000 square degrees. Putting the galaxy distribution Eq. (4.1) and bias Eq. (4.2) plotted in Fig. 1 back into the log-likelihood estimator in Eq. (3.8), we obtain the total SNR as a function of the lightest neutrino mass  $m_\nu^{\text{lightest}} \equiv m_1$  (NO) and  $m_\nu^{\text{lightest}} \equiv m_3$  (IO) as blue and red lines, respectively, in Fig. 4. In our calculations, we take the neutrino mass squared differences to be  $\Delta m_{21}^2 = 7.54 \times 10^{-5} \text{ eV}^2$ ,  $\Delta m_{31}^2 = 2.47 \times 10^{-3} \text{ eV}^2$  [7].

The left panel of Fig. 4 displays the SNR varying with the lightest neutrino mass  $m_\nu^{\text{lightest}}$ , for the BGS only (dashed) and the combination of all categories (solid). For comparison, the current constraint ( $\sum m_i < 0.13$  eV at 95% C.L.) by combining both cosmology [67] and neutrino oscillation [7] has been shown as shaded regions for both NO (blue) and IO (red). We can see that the projected sensitivity of cosmic gravitational focusing at DESI with only BGS (blue dashed) can already significantly exceed the existing one. After including the faint galaxies (solid), the total SNR can further increase by 20%. The 95% upper limit on the lightest neutrino mass can reach  $m_\nu^{\text{lightest}} = m_1 < 0.016$  eV for NO while the current one is 0.034 eV. For IO, the vanishing lightest mass is even beyond  $2\sigma$ . In other words, the IO scenario with vanishing lightest mass is possible to be excluded with cosmic gravitational focusing by more than  $2\sigma$  at DESI while the current constraint can only reach around 0.02 eV. Including the cosmic gravitational focusing as a third independent cosmological constraint, in addition to CMB and LSS, on the neutrino mass is of profound significance.

From NO (blue) to IO (red), the SNR increases by roughly a factor of 2 since IO has two nearly degenerate heavy neutrino masses while NO has only one heavy mass. As emphasized in the previous sections, the gravitational focusing effect has fourth power dependence on the neutrino masses. Heavy neutrinos leaves much more significant effect in the cosmic gravitational focusing.

The right panel of Fig. 4 shows the synergy of the cosmic gravitational focusing and the current constraints. We can see that the left side of the shaded regions corresponds to the 95% C.L. value of the dotted lines. After combination with the projected sensitivity of DESI gravitational focusing observation (dot-dashed), the vanishing lightest mass scenario with IO (red) can be excluded up to almost  $3\sigma$ . Even for the case of NO (blue), the upper limit can further enhance to  $m_{\text{lightest}} < 3.2$  meV at 95% C.L.

Future galaxy surveys will further improve the existing CMB and LSS constraints on the neutrino mass sum. For example, the CSST [126–129] will be able to reach  $\sigma_{\sum m_i} \sim 0.23$  eV [130]. In addition, DESI-II [131] and Subaru PFS [132] can reach  $\sigma_{\sum m_i} \sim 0.02$  eV, and  $\sigma_{\sum m_i} \sim 0.03$  eV at EUCLID [133] for NO, in combination with the Planck 2018 data. For the adopted mass sum,  $\sum m_i = 0.125$  eV, the combination of future LSS with Planck 2018 will reach  $\sigma_{\sum m_i} = 0.03$  eV for NO ( $m_3 = 0.125$  eV,  $m_1 \approx m_2 \approx 0$ ) and  $\sigma_{\sum m_i} = 0.04$  eV for IO ( $m_1 \approx m_2 \approx 0.0625$  eV,  $m_3 \approx 0$ ) (See Table 5 of [134]). It is interesting to notice that the combination of CMB and LSS observations has better sensitivity for NO than IO due to the free-streaming effect [135]. For the mass sum  $\sum m_i = 0.125$  eV adopted above, the heaviest neutrino mass ( $m_3 = 0.125$  eV) for NO is nearly twice the one ( $m_1 \approx m_2 \approx 0.0625$  eV) for IO. With a larger mass, the NO neutrino becomes non-relativistic earlier and suppresses the power spectrum at small scales. Consequently, the NO constraint is stronger than the IO one. Note that these experimental sensitivities are estimated for the smallest neutrino mass scenario with  $m_\nu^{\text{lightest}} = 0$ . For nonzero lightest neutrino mass and hence larger mass sum to be measured, its uncertainty  $\sigma_{\sum m_i}$  is expected to become smaller with a larger observable. As a conservative comparison, we take



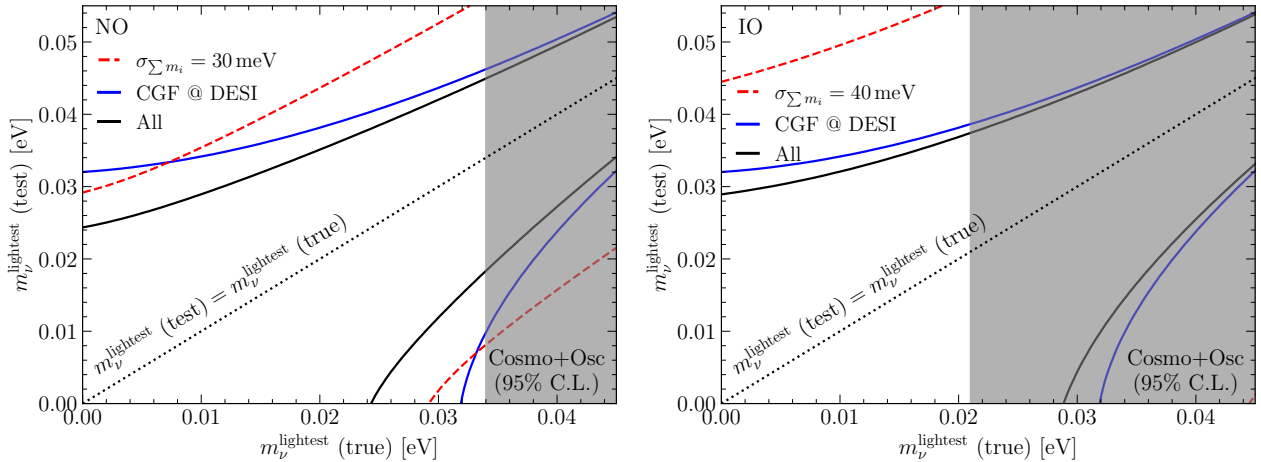


Fig. 5: The upper and lower limits on the lightest neutrino mass for NO (left) and IO (right). While the black dotted line stands for the central value, namely the test value being the same as the true one, the lines above it indicate the upper limits and those below the lower limits at 95% C.L.. The future cosmological observations ( $\sigma_{\Sigma m_i} = 30$  (40) meV for NO (IO) from CMB and LSS [133]) are shown as red dashed lines, the projected DESI sensitivity with cosmic gravitational focusing (CGF) as blue solid lines, and their combination as black solid lines. For comparison, the combination of existing cosmological constraints and neutrino oscillation experiments at 95% C.L. [7] are shown with grey filled region.

these nominal values of projected uncertainties universally for a tunable lightest neutrino mass to make illustration in Fig. 5. A perfect observation falls on the black dotted line  $m_{\nu}^{\text{lightest}}(\text{test}) = m_{\nu}^{\text{lightest}}(\text{true})$  while the distance from this line represents the 95% C.L. uncertainty for a given  $m_{\nu}(\text{true})$ . Larger distance means larger uncertainty. We can see that the other cosmological constraints (red dashed) still span a wide range around the true values (black dotted) even after taking the projected sensitivities from future observations. This is especially true for the IO (right) as well as the NO (left) in most of the parameter space.

For the cosmic gravitational focusing constraint (blue solid) in Fig. 5, its sensitivity is estimated by replacing the signal strength in Eq. (3.6) with the signal difference,  $\mathcal{S} \rightarrow \mathcal{S}_{\text{true}} - \mathcal{S}_{\text{test}}$ , where  $\mathcal{S}_{\text{true}}$  ( $\mathcal{S}_{\text{test}}$ ) is obtained with the true (test) neutrino mass parameter. It is worth noticing that the uncertainty decreases with increasing true neutrino mass since a larger mass provides a larger signal and hence easier to be measured as we already pointed out above. Comparing with the other constraints (red dashed), the gravitational focusing measurement is particularly good for larger mass. Namely, the blue solid lines shrink towards the central values (black dotted) much faster than the red dashed lines. This is because the cosmic gravitational focusing has fourth power dependence on the neutrino masses as we emphasized above while the conventional ways have only linear dependence. This trend is even more prominent for the IO case in the right panel with two heavy neutrinos. It fully demonstrates the advantage of cosmic gravitational focusing as an extra and independent cosmological measurement of the neutrino masses.

The synergy (black solid) of cosmic gravitational focusing and other cosmological constraints



significantly improve the upper and lower limits across the whole parameter space. Especially, the intersection of the lower limit curve with the horizontal axis can move below 30 meV. In other words, it is possible to put a lower limit on the lightest neutrino mass at 95% C.L. for true values down to 24 meV (29 meV) with NO (IO). Below that, only upper limit is possible which can be as small as 25 meV (29 meV) for NO (IO) when the lightest mass approaches 0. These features apply for both NO (left) and IO (right) with slightly different values. For comparison, the 95% upper limit from the combination (grey region) of existing cosmological observations and neutrino oscillation experiments is also shown.

## 6. Conclusions

Under the gravitational force of DM overdensity, the  $C\nu F$  can experience gravitational lensing which has two phenomenological consequences of dynamical friction and gravitational focusing. While the dynamical friction is mainly the drag force between  $C\nu F$  and DM halo, the gravitational focusing directly leads to a  $C\nu F$  density enhancement on the downstream side of the DM halo. This one-sided density enhancement is essentially a dipole component after subtracting the average density. Since the  $C\nu F$  density can also contribute to the total matter density, the dipole structure can manifest itself in the galaxy distribution as an imaginary galaxy cross correlation in the Fourier space. It is much more intuitive and appropriate to use cosmic gravitational focusing to name this effect.

We use both single-particle trajectory with general relativity for point source of gravitational potential and Boltzmann equation formalism for continuous overdensities to describe the cosmic gravitational focusing. Our results apply for both relativistic and non-relativistic particles with dependence on the fourth power of mass and temperature. While the CMB photons have negligible effect with vanishing mass, the cosmic gravitational focusing mainly comes from  $C\nu F$  with at least one heavy mass. The cosmic gravitational focusing can then serve as an independent way of measuring the neutrino masses.

When deriving the galaxy cross correlation, we keep the most general form of bias for both  $C\nu F$  and DM overdensities. Since  $C\nu F$  and DM have different clustering properties, it makes much more sense for them to have different bias. More specifically, the  $C\nu F$  bias is very close to 1 with only  $\lesssim 2\%$  deviation. This allows two different RSD terms that add up coherently to enhance the cosmic gravitational focusing effect in the galaxy cross correlation. With this enhancement, the cosmic gravitational focusing provides a more powerful way of determining the neutrino masses than the mass sum constraint. Since observing the dipole density distribution requires galaxy cross correlation among categories with different bias, we split the BGS galaxies into two sub-categories and find the optimal mass splitting value to maximize the SNR.

Finally, we quantitatively show the advantages of cosmic gravitational focusing by taking the

projected sensitivity at DESI as an illustration. The SNR can improve by at least a factor of 2 after incorporating the DESI gravitational focusing measurement to the existing cosmological constraints from CMB and LSS. Especially the vanishing lightest neutrino mass with IO can be excluded up to almost  $3\sigma$  and the upper limit on the lightest neutrino mass can touch down to 3.2 meV at 95% C.L. for NO as shown in Fig. 4. Even for the projected sensitivity of CMB and LSS observations at CSST, DESI-II, EUCLID, and Subaru PFS, the cosmic gravitational focusing sensitivity is still very competitive as summarized in Fig. 5. A lower bound is possible for smaller lightest mass than the other ways. Its advantage is more significant for heavier neutrinos with fourth power dependence on the neutrino mass.

## Acknowledgements

The authors would like to thank Xiao-Hu Yang and Hong-Ming Zhu for useful discussions. The authors are supported by the National Natural Science Foundation of China (12375101, 12090060, 12090064, and 12247141) and the SJTU Double First Class start-up fund (WF220442604). SFG is also an affiliate member of Kavli IPMU, University of Tokyo. PSP is also supported by the Grant-in-Aid for Innovative Areas No. 19H05810.

## A. $C\nu F$ -DM Relative Velocity and Its Dispersion

The crucial factor of cosmic gravitational focusing, namely the relative velocity between  $C\nu F$  and DM halo, is developed in the evolution of early Universe. In the presence of matter density fluctuations, the cosmic neutrinos fall into the gravitational potential well and obtain a relative velocity. It is then necessary to first estimate the overdensity fluctuation and the relative velocity therein as we elaborate in this appendix.

With perturbative overdensity in the early Universe, the linear approximation [72] can apply. As the primordial fluctuations usually follow gaussian distribution, the ensemble average of the relative velocity alone should vanish,  $\langle \mathbf{v}_{\nu c} \rangle = 0$ . In addition, the Universe is homogeneous and isotropic at large scales which means the relative velocity should appear at small scales. Especially, cosmic neutrinos and DM have a distinct thermal history which allows a non-zero relative velocity at scales below  $\sim 100$  Mpc [72, 73]. Since 100 Mpc is already quite sizable, the  $C\nu F$ -DM relative velocity distribution can be decomposed into a background (or bulk) velocity  $\mathbf{v}_{\nu c}^{\text{bg}}$  and small perturbations  $\mathbf{u}_{\nu c}(\mathbf{x}) \equiv \mathbf{v}_{\nu c} - \mathbf{v}_{\nu c}^{\text{bg}}$  at even smaller scales. The small perturbations around the bulk velocity  $\mathbf{v}_{\nu c}^{\text{bg}}$  are isotropic  $\langle \mathbf{u}_{\nu c}(\mathbf{x}) \rangle = 0$  and the relative velocity dispersion can be estimated by the background bulk velocity,  $\sqrt{\langle \mathbf{v}_{\nu c}^2 \rangle} = \sqrt{\langle (\mathbf{v}_{\nu c}^{\text{bg}})^2 \rangle} + \mathcal{O}(\mathbf{u}_{\nu c}^2) \approx v_{\nu c}^{\text{bg}}$ .

We estimate the background velocity as the root-mean-square of the relative velocity field

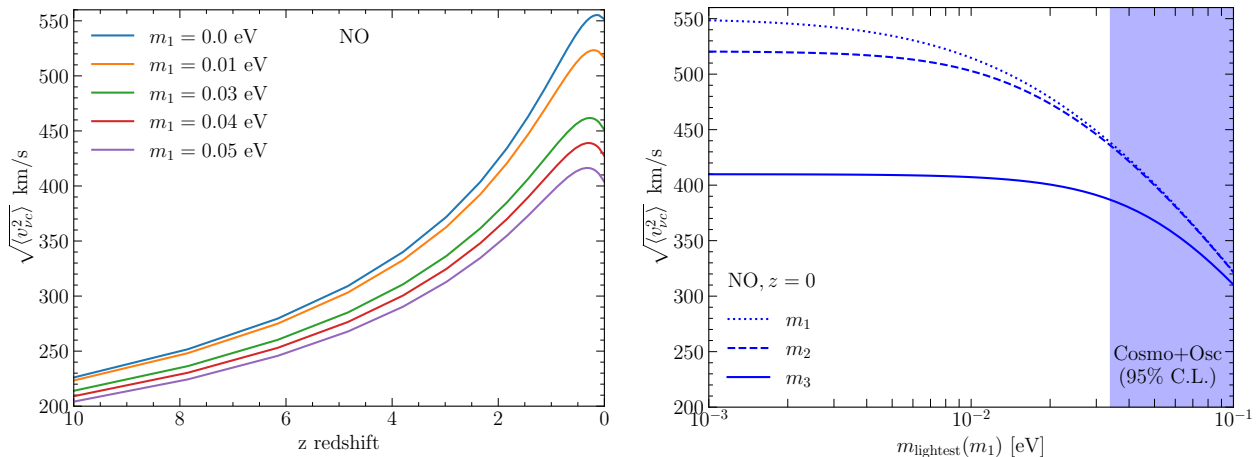


Fig. 6: (Left) The relative velocity between  $C\nu F$  and DM for the lightest mass  $m_1$  in the NO as a function of redshift  $z$ . (Right) The relative velocities for the three massive neutrinos as functions of the lightest neutrino mass ( $m_{\text{lightest}} = m_1$  for NO) at nowadays ( $z = 0$ ).

[72, 73],

$$v_{\nu c}^{\text{bg}} \approx \langle \mathbf{v}_{\nu c}^2(R) \rangle = \int \frac{d|\mathbf{k}|}{|\mathbf{k}|} \Delta_{\zeta}^2(\mathbf{k}) \left| \widetilde{W}(|\mathbf{k}|R) \right|^2 \frac{|T_{\theta_{\nu}} - T_{\theta_c}|^2}{|\mathbf{k}|^2}, \quad (\text{A.1})$$

where the primordial power spectrum  $\Delta_{\zeta}$  and transfer function of the velocity divergence  $T_{\theta_a} \equiv \tilde{\theta}_a/\zeta$  ( $a = \nu, c$ ) can be obtained from the CLASS code [136] with the Planck 2018 best fit [67]. The top-hat window function  $\widetilde{W}(|\mathbf{k}|R)$  selects those scales smaller than  $R$ .

Since the cosmic gravitational focusing is proportional to the relative velocity, a larger velocity increases the signal. At the same time, the velocity becomes larger for smaller filtering scale  $R$  [73] and the signal becomes optimal for smaller  $R$ . However, the average distance between two nearest galaxies is 2 Mpc [137]. To observe the effect of cosmic gravitational focusing on the dipole galaxy distribution, it is necessary for the window function to cover neighboring galaxies with radius  $R \gtrsim 2$  Mpc. In addition, the nonlinear effect would become important below  $R = |\mathbf{k}|^{-1} \sim 5 \text{ Mpc}/h$  [39]. In order to use the power spectrum simulated in the linear regime with typical code such as CLASS [136], the window function radius cannot be too small. A reasonable choice is  $R = 5 \text{ Mpc}/h$ .

In the left panel of Fig. 6, we show how the relative velocity changes with redshift  $z$  for different neutrino masses. The relative velocity is larger for smaller masses and increases with redshift until it reaches around  $z \sim 0.4$ . As explained earlier, the  $C\nu B$  neutrinos fall into the gravitational potential of mass density fluctuations and obtain a relative velocity. Since the matter clustering increases with the Universe evolution, or equivalently decreasing redshift, the  $C\nu B$ -DM relative velocity also increases and finally reaches (400 ~ 500) km/s. After that, the dark energy (DE) starts to dominate and the relative velocity decreases since DE can resist the clustering tendency.

For the degenerate case, three neutrinos have the roughly same relative velocity [72]. But for

the real case, the three neutrinos could have different bulk velocities. To show this difference, we take the NO for example in the right panel of Fig. 6. Since the lightest neutrino (solid blue) has a larger velocity dispersion of  $v_{\nu c} \propto \sum \int p_{\nu}/m_{\nu}$  than that of the two heavy ones (dashed and dotted blue), it has a relative velocity about 40% larger. In this region, the mass squared differences,  $m_2 \approx \sqrt{\Delta m_{21}^2}$  and  $m_3 \approx \sqrt{\Delta m_{31}^2}$ , dominate over the lightest mass  $m_{\text{lightest}}$ . So varying the tiny  $m_{\text{lightest}}$  has negligible effect and the curves are almost flat. As the lightest neutrino mass increases, the two light neutrino masses  $m_1$  and  $m_2$  become degenerate first as manifested by the converging dotted and dashed lines. With further increasing mass, once the lightest mass surpasses the larger mass squared difference,  $m_{\text{lightest}} = m_1 > \sqrt{\Delta m_{31}^2} \approx 0.05$  eV, all the masses become degenerate,  $m_1 \approx m_2 \approx m_3$ . This explains why the three neutrinos converge on the right-hand side with roughly the same velocity around 300 km/s. In all cases, the background neutrino velocities are nonrelativistic and of order  $\sqrt{\langle v_{\nu c}^2 \rangle} \sim \mathcal{O}(100)$  km/s. Most importantly, the velocity dispersion decreases with the neutrino mass. This is because the C $\nu$ F and DM relative velocity have been implemented [138] in the CLASS [136], CAMB [139], CMBEASY [140], and CMBFAST [141] packages. Although not emphasized, the cosmic dynamical friction has already been existing in the early Universe simulations. With larger mass, the drag force between C $\nu$ F and matter overdensity is also larger to reduce the relative velocity.

## B. Neutrino Dipole Density Distribution Induced by Anisotropic Phase Space Distribution

The C $\nu$ F has non-zero velocity relative to the DM halo. As shown in Fig. 6, this relative velocity  $|\mathbf{v}_{\nu c}| \approx 10^{-3}$  (100 km/s) is non-relativistic even if individual neutrinos can be relativistic. We can perform Lorentz boost from the C $\nu$ F frame ( $\mathbf{p}'$ ) to the DM frame ( $\mathbf{p}$ ). When expanded to the linear order of  $\mathbf{v}_{\nu c}$ , the cosmic neutrino momentum and energy transform as,

$$\mathbf{p} \approx \mathbf{p}' + E_{\mathbf{p}'} \mathbf{v}_{\nu c}, \quad \text{and} \quad E_{\mathbf{p}} \approx E_{\mathbf{p}'} + \mathbf{p}' \cdot \mathbf{v}_{\nu c}. \quad (\text{B.1})$$

As a result, the isotropic cosmic neutrino phase-space distribution function in the C $\nu$ F frame receives anisotropic correction to become  $f_{\nu}(\mathbf{p}_i, \mathbf{v}) \approx 2 / (e^{|\mathbf{p}_i - E_{\mathbf{p}_i} \mathbf{v}_{\nu c}|/T} + 1)$  in the DM frame as summarized in Eq. (2.8). The prefactor 2 denotes the equal contributions of neutrino and anti-neutrino for the same mass eigenstate. To make the effect of C $\nu$ F-DM relative velocity  $\mathbf{v}_{\nu c}$  explicit, it is better to expand to the linear order of  $\mathbf{v}_{\nu c}$ . With a nonrelativistic Lorentz boost  $|\mathbf{v}_{\nu c}| \sim 10^{-3}$  as shown in Fig. 6, the correction to the matter density is essentially a Lorentz boost factor  $\gamma \equiv \sqrt{1 - |\mathbf{v}_{\nu c}|^2}$  which only gives a factor of  $10^{-6}$  difference. So it is safe to work in the DM frame.

Below we show the detailed derivations to fill the gap between Eq. (2.14) and Eq. (2.15). First, we need to perform the momentum gradient  $\nabla_{\mathbf{p}}$  on the homogeneous part  $\bar{f}_{\nu}(\mathbf{p})$  of the

neutrino phase space distribution function,

$$\frac{\partial \bar{f}_\nu(\mathbf{p})}{\partial p_j} = \frac{\partial p'_i}{\partial p_j} \frac{\partial \bar{f}_\nu(|\mathbf{p}'|)}{\partial p'_i} = \frac{\partial p'_i}{\partial p_j} \hat{p}'_i \frac{d\bar{f}_\nu(|\mathbf{p}'|)}{d|\mathbf{p}'|}. \quad (\text{B.2})$$

Using the Lorentz transformation in Eq. (B.1), the first derivative can be written in terms of the neutrino momentum and energy,  $\partial p'_i / \partial p_j \approx \delta_{ij} - p_j v_{\nu ci} / E_{\mathbf{p}} \approx \delta_{ij} - p'_j v_{\nu ci} / E_{\mathbf{p}'}$ . Putting things together, the momentum gradient becomes,

$$\nabla_{\mathbf{p}} \bar{f}_\nu(\mathbf{p}) \approx \hat{\mathbf{p}}' \left( 1 - \frac{\mathbf{v}_{\nu c} \cdot \mathbf{p}'}{E_{\mathbf{p}'}} \right) \frac{d\bar{f}_\nu(|\mathbf{p}'|)}{d|\mathbf{p}'|}. \quad (\text{B.3})$$

To implement the Lorentz transformation, one may first use Eq. (B.1) and Eq. (B.3) to replace the neutrino momentum  $\mathbf{p}$  (also  $E_{\mathbf{p}}$ ) and its gradient in Eq. (2.14),

$$\begin{aligned} \delta \tilde{\rho}_\nu \approx & \tilde{\Psi} \int \frac{d^3 \mathbf{p}'}{(2\pi)^3} E_{\mathbf{p}'} \left( 1 + \frac{\mathbf{p}' \cdot \mathbf{v}_{\nu c}}{E_{\mathbf{p}'}} \right) \\ & \times \left\{ \frac{m_\nu^2 + 2|\mathbf{p}'|^2 + 4E_{\mathbf{p}'}(\mathbf{p}' \cdot \mathbf{v}_{\nu c})}{(\mathbf{p}' + E_{\mathbf{p}'} \mathbf{v}_{\nu c}) \cdot \mathbf{k}} \mathbf{k} \cdot \hat{\mathbf{p}}' - \left[ |\mathbf{p}'| + E_{\mathbf{p}'}(\mathbf{v}_{\nu c} \cdot \hat{\mathbf{p}}') \right] \right\} \frac{d\bar{f}_\nu(|\mathbf{p}'|)}{d|\mathbf{p}'|}, \end{aligned} \quad (\text{B.4})$$

where the integration variable has also been replaced accordingly,  $d^3 \mathbf{p} / E_{\mathbf{p}} = d^3 \mathbf{p}' / E_{\mathbf{p}'}$ . It is much more convenient to see the features by combining the two terms in the curly bracket and extracting the denominator as an overall factor,

$$\delta \tilde{\rho}_\nu \approx \tilde{\Psi} \int \frac{d^3 \mathbf{p}'}{(2\pi)^3} \frac{d\bar{f}_\nu}{d|\mathbf{p}'|} \frac{E_{\mathbf{p}'}}{(\mathbf{p}' + E_{\mathbf{p}'} \mathbf{v}_{\nu c}) \cdot \mathbf{k}} \left\{ \mathbf{k} \cdot \hat{\mathbf{p}}' + \frac{|\mathbf{p}'|}{E_{\mathbf{p}'}} \left[ 4(\hat{\mathbf{p}}' \cdot \mathbf{v}_{\nu c})(\mathbf{k} \cdot \hat{\mathbf{p}}') - (\mathbf{v}_{\nu c} \cdot \mathbf{k}) \right] \right\}. \quad (\text{B.5})$$

Of the three terms in the curly bracket, the first one dominates for non-relativistic neutrinos  $E_{\mathbf{p}'} \gg |\mathbf{p}'|$  while the second term is suppressed by  $|\mathbf{p}'|/E_{\mathbf{p}'}$ .

Since the relative bulk velocity  $\mathbf{v}_{\nu c}$  is non-relativistic, the denominator can vanish and lead to a divergence which can be replaced by a  $\delta$ -function using the SPW theorem [94],

$$\frac{1}{(\mathbf{p}' + E_{\mathbf{p}'} \mathbf{v}_{\nu c}) \cdot \mathbf{k}} \Rightarrow \mathcal{P} \left( \frac{1}{(\mathbf{p}' + E_{\mathbf{p}'} \mathbf{v}_{\nu c}) \cdot \mathbf{k}} \right) + i\pi \delta(\mathbf{p}' \cdot \mathbf{k} + E_{\mathbf{p}'} \mathbf{v}_{\nu c} \cdot \mathbf{k}). \quad (\text{B.6})$$

For given bulk velocity  $\mathbf{v}_{\nu c}$  and comoving wave number  $\mathbf{k}$ , the argument of the  $\delta$ -function depends on the opening angle between  $\mathbf{p}'$  and  $\mathbf{k}$ . It is then more convenient to rewrite the integration  $d^3 \mathbf{p}' = |\mathbf{p}'|^2 d|\mathbf{p}'| d\Omega_{\mathbf{p}'}$  in terms of its solid angle. Then the  $\delta$ -function can be rewritten in terms of opening angles,  $\delta(|\mathbf{p}'||\mathbf{k}| \cos \theta + E_{\mathbf{p}'} \mathbf{v}_{\nu c} \cdot \mathbf{k}) = \delta(\cos \theta - \cos \theta_0) / |\mathbf{p}'||\mathbf{k}|$  with  $\cos \theta_0 \equiv -(\mathbf{v}_{\nu c} \cdot \hat{\mathbf{k}}) / |\mathbf{v}'|$ . Note that  $\mathbf{v}' \equiv |\mathbf{p}'|/E_{\mathbf{p}'}$  is the velocity of individual neutrino in the C $\nu$ F frame. The integration over  $\delta$ -function is non-zero only if  $|\mathbf{p}'| > E_{\mathbf{p}'} |\mathbf{v}_{\nu c} \cdot \hat{\mathbf{k}}|$ . It is interesting to see this gives an imaginary part to the neutrino density distribution in the momentum space,

The  $\mathbf{k} \cdot \hat{\mathbf{p}}'$  in the first two terms of Eq. (B.5) has been replaced by  $-(\mathbf{v}_{\nu c} \cdot \mathbf{k})/|\mathbf{v}'|$  due to the  $\delta$ -function.

$$\text{Im}[\delta \rho_\nu] = -\frac{\tilde{\Psi}}{8\pi^2} \int d|\mathbf{p}'| |\mathbf{p}'|^2 E_{\mathbf{p}'}^3 \frac{d\bar{f}}{d|\mathbf{p}'|} \Theta(|\mathbf{p}'| - E_{\mathbf{p}'} |\mathbf{v}_{\nu c} \cdot \hat{\mathbf{k}}|)$$

$$\times \frac{2\pi}{|\mathbf{p}'||\mathbf{k}|} \left[ \frac{E_{\mathbf{p}'}}{|\mathbf{p}'|} (\mathbf{v}_{\nu c} \cdot \mathbf{k}) + 4 \frac{E_{\mathbf{p}'}}{|\mathbf{p}'|} (\mathbf{v}_{\nu c} \cdot \hat{\mathbf{k}})^3 |\mathbf{k}| + \frac{|\mathbf{p}'|}{E_{\mathbf{p}'}} (\mathbf{v}_{\nu c} \cdot \mathbf{k}) \right]. \quad (\text{B.7})$$

Although the first two terms share the same  $E_{\mathbf{p}'}/|\mathbf{p}'|$  factor, the second one is suppressed by  $v_{\nu c}^3$  and hence can be omitted for simplicity. The remaining two terms can be comparable for relativistic neutrinos. The inner product  $\mathbf{v}_{\nu c} \cdot \mathbf{k}$  can be extracted as an overall factor to give a much simpler form,

$$\text{Im}[\delta\rho_\nu] = -\frac{\tilde{\Psi}(\mathbf{v}_{\nu c} \cdot \hat{\mathbf{k}})}{4\pi} \int d|\mathbf{p}'| (m_\nu^4 + 3m_\nu^2 |\mathbf{p}'|^2 + 2|\mathbf{p}'|^4) \frac{d\bar{f}}{d|\mathbf{p}'|} \Theta(|\mathbf{p}'| - E_{\mathbf{p}'} |\mathbf{v}_{\nu c} \cdot \hat{\mathbf{k}}|). \quad (\text{B.8})$$

Similar to the classical picture with a point source of gravitational potential, the cosmic gravitational focusing also relies on the fourth power of neutrino mass  $m_\nu$  and its momentum  $\mathbf{p}'$ . The non-relativistic neutrino case is dominated by the mass  $m_\nu^4$  while the relativistic case by the neutrino momentum.

The momentum integration will give the dependence on the neutrino temperature  $T_\nu$ . Note that the integration range is determined by the  $\Theta(|\mathbf{p}'| - E_{\mathbf{p}'} |\mathbf{v}_{\nu c} \cdot \hat{\mathbf{k}}|)$  which means  $|\mathbf{p}'| > m_\nu |\mathbf{v}_{\nu c} \cdot \hat{\mathbf{k}}| / \sqrt{1 - (\mathbf{v}_{\nu c} \cdot \hat{\mathbf{k}})^2} \approx m_\nu |\mathbf{v}_{\nu c} \cdot \hat{\mathbf{k}}|$ . The integration in Eq. (2.20) can be generally parametrized as,

$$\int d|\mathbf{p}'| |\mathbf{p}'|^{2n} \frac{d\bar{f}}{d|\mathbf{p}'|} \Theta(|\mathbf{p}'| - E_{\mathbf{p}'} |\mathbf{v}_{\nu c} \cdot \hat{\mathbf{k}}|) = 2T_\nu^{2n} \int_{y_0}^{\infty} dy y^{2n} \frac{d[e^y + 1]^{-1}}{\partial y} \equiv T_\nu^{2n} f_n(y_0), \quad (\text{B.9})$$

by performing a variable change  $y \equiv |\mathbf{p}'|/T_\nu$  with  $y_0 \equiv m_\nu |\mathbf{v}_{\nu c} \cdot \hat{\mathbf{k}}|/T_\nu$ . The factor 2 comes from the phase space distribution function to account for both neutrino and antineutrino contributions. For convenience, we have defined three handy functions  $f_n(y_0)$  ( $n = 1, 2, 3$ ),

$$f_n(y_0) \equiv 2 \int_{y_0}^{\infty} dy y^{2n} \frac{d[e^y + 1]^{-1}}{\partial y} = - \int_{y_0}^{\infty} dy y^{2n} \frac{1}{1 + \cosh y}. \quad (\text{B.10})$$

Finally, Eq. (B.8) can be written as,

$$\text{Im}[\delta\rho_\nu] = -\frac{\tilde{\Psi}}{4\pi} \sum_i (\mathbf{v}_{\nu c} \cdot \hat{\mathbf{k}}) [m_i^4 f_0 + 3m_i^2 T_\nu^2 f_1 + 2T_\nu^4 f_2], \quad (\text{B.11})$$

where we have summed over the three mass eigenstates. The same procedure is also applied from Eq. (2.20) to Eq. (2.22). The equal contributions of neutrino and antineutrino for the same mass eigenstate has been taken into account by the factor of 2 intrinsically defined in the neutrino phase space distribution functions at the beginning of this appendix.

The largest  $y_0 \approx 0.5$  happens for  $m_3 \lesssim 0.07 \text{ eV}$  (NO for  $\sum m_i = 0.13 \text{ eV}$ ) when  $T_\nu \sim 1.7 \times 10^{-4} \text{ eV}$ . The function  $f_n(y_0)$  can be expanded as power series of  $y_0$ ,

$$f_0(y_0) \approx -1 + \frac{y_0}{2} + \mathcal{O}(y_0^3), \quad f_1(y_0) \approx -\frac{\pi^2}{3} + \mathcal{O}(y_0^3), \quad \text{and} \quad f_2(y_0) \approx -\frac{7\pi^4}{15} + \mathcal{O}(y_0^5). \quad (\text{B.12})$$

For  $f_0$ , we preserve the linear order of  $\mathcal{O}(y_0)$ , since the difference between  $-1 + y_0/2$  and  $-1$  is almost 25% for the largest  $y_0 \approx 0.5$ . The next order  $\mathcal{O}(y_0^3)$  correction is smaller than 0.7% and

can be safely ignored. With such an approximation, Eq. (B.11) becomes,

$$\text{Im}[\delta\rho_\nu] = \frac{\tilde{\Psi}}{4\pi} \sum_i (\mathbf{v}_{\nu c} \cdot \hat{\mathbf{k}}) \left[ m_i^4 \left( 1 - \frac{m_i |\mathbf{v}_{\nu c} \cdot \hat{\mathbf{k}}|}{2T_\nu} \right) + \pi^2 m_i^2 T_\nu^2 + \frac{14}{15} \pi^4 T_\nu^4 \right]. \quad (\text{B.13})$$

For the second term in the parenthesis, the non-relativistic C $\nu$ F-DM relative velocity is amplified by the prefactor,  $m_1/2T_\nu \approx \mathcal{O}(100)$ . The gravitational potential  $\tilde{\Psi}$  is generated mainly by matter and hence should be replaced by the matter density,  $\tilde{\Psi} = -4\pi G a^2 \rho_m \tilde{\delta}_{m0}/|\mathbf{k}|^2$ , according to the gravitational Poisson equation.

## C. Imaginary Density Fluctuation as Ensemble Average of Primordial Power Spectrum

The neutrino energy density also contributes to the total matter overdensity  $\tilde{\delta}_m \equiv \tilde{\delta}_{m0}(1 + i\tilde{\phi})$ , as mentioned in Sec. 2.2.2. Starting from Eq. (2.23) whose derivation details have been provided in the previous App. B, the imaginary overdensity can be parametrized as a phase shift to the matter overdensity,

$$\tilde{\phi}_i \equiv -\frac{a^2}{|\mathbf{k}|^2} (\mathbf{v}_{\nu c} \cdot \hat{\mathbf{k}}) \left( \beta_i - \alpha_i |\mathbf{v}_{\nu c} \cdot \hat{\mathbf{k}}| \right), \quad (\text{C.1})$$

where we define two coefficients  $\beta_i$  and  $\alpha_i$ ,

$$\beta_i \equiv G \left( m_i^4 + \pi^2 m_i^2 T_\nu^2 + \frac{14}{15} \pi^4 T_\nu^4 \right), \quad \alpha_i \equiv G \frac{m_i^5}{2T_\nu}, \quad (\text{C.2})$$

for simplicity. While the  $\beta_i$  term associated with a linear  $\mathbf{v}_{\nu c} \cdot \hat{\mathbf{k}}$  captures the main contributions from the neutrino mass eigenstate with mass  $m_i$ , the  $\alpha_i$  term has quadratic dependence on  $\mathcal{O}(\mathbf{v}_{\nu c}^2)$ . In other words, the  $\alpha_i$  term originates from the  $m_i |\mathbf{v}_{\nu c} \cdot \hat{\mathbf{k}}|/2T_\nu$  term of Eq. (B.13). Since the largest mass is at least  $m_1(m_3) \gtrsim 0.05$  eV while the neutrino temperature nowadays is around  $10^{-4}$  eV,  $\alpha_i/\beta_i \approx m_i/2T_\nu \gtrsim 250$  and  $\alpha_i v_{\nu c}/\beta_i \gtrsim 0.25$ . The  $\alpha_i$  term can contribute at least 25% for the heaviest neutrino and it is necessary to expand to the second order of the  $\alpha_i$  terms.

Putting Eq. (C.1) back, the two ensemble averages  $\langle \tilde{\phi}_i^2 \rangle$  and  $\langle \dot{\tilde{\phi}}_i^2 \rangle$  in Eq. (3.9) are,

$$\langle \tilde{\phi}_i^2 \rangle = \frac{a^4}{|\mathbf{k}|^4} \langle (\mathbf{v}_{\nu c} \cdot \hat{\mathbf{k}})^2 \rangle \left[ \beta_i^2 - \frac{4\sqrt{2}}{\sqrt{\pi}} \alpha_i \beta_i \sqrt{\langle (\mathbf{v}_{\nu c} \cdot \hat{\mathbf{k}})^2 \rangle} + 3\alpha_i^2 \langle (\mathbf{v}_{\nu c} \cdot \hat{\mathbf{k}})^2 \rangle \right], \quad (\text{C.3a})$$

$$\begin{aligned} \frac{\langle \dot{\tilde{\phi}}_i^2 \rangle}{H^2} &= \frac{a^2 \beta_i^2}{|\mathbf{k}|^4} \left[ 4a^2 \langle (\mathbf{v}_{\nu c} \cdot \hat{\mathbf{k}})^2 \rangle - 4a \langle (\mathbf{v}_{\nu c} \cdot \hat{\mathbf{k}}) \partial_z (\mathbf{v}_{\nu c} \cdot \hat{\mathbf{k}}) \rangle + \langle [\partial_z (\mathbf{v}_{\nu c} \cdot \hat{\mathbf{k}})]^2 \rangle \right] - \frac{4\sqrt{2} a^2 \beta_i \alpha_i}{\sqrt{\pi} |\mathbf{k}|^4} \\ &\quad \times \left[ 6a^2 \langle (\mathbf{v}_{\nu c} \cdot \hat{\mathbf{k}})^2 \rangle - 7a \langle (\mathbf{v}_{\nu c} \cdot \hat{\mathbf{k}}) \partial_z (\mathbf{v}_{\nu c} \cdot \hat{\mathbf{k}}) \rangle + 2 \langle [\partial_z (\mathbf{v}_{\nu c} \cdot \hat{\mathbf{k}})]^2 \rangle \right] \sqrt{\langle (\mathbf{v}_{\nu c} \cdot \hat{\mathbf{k}})^2 \rangle} \\ &\quad + \frac{a^2 \alpha_{\nu j}^2}{|\mathbf{k}|^4} \left\{ 27a^2 \langle (\mathbf{v}_{\nu j c} \cdot \hat{\mathbf{k}})^2 \rangle^2 - 36a \langle (\mathbf{v}_{\nu j c} \cdot \hat{\mathbf{k}})^2 \rangle \langle (\mathbf{v}_{\nu j c} \cdot \hat{\mathbf{k}}) \partial_z (\mathbf{v}_{\nu j c} \cdot \hat{\mathbf{k}}) \rangle \right\} \end{aligned}$$



$$+ 4 \left\langle (\mathbf{v}_{\nu_{jc}} \cdot \hat{\mathbf{k}})^2 \right\rangle \left\langle [\partial_z (\mathbf{v}_{\nu_{jc}} \cdot \hat{\mathbf{k}})]^2 \right\rangle + 8 \left\langle (\mathbf{v}_{\nu_{jc}} \cdot \hat{\mathbf{k}}) [\partial_z (\mathbf{v}_{\nu_{jc}} \cdot \hat{\mathbf{k}})] \right\rangle^2, \quad (\text{C.3b})$$

where  $\partial_z$  is the redshift derivative. For the heavy neutrino case with  $m_i \gg T_\nu$ , the  $\alpha_i$  and  $\beta_i$  parameters have hierarchical structure,  $\alpha_i = \dot{\alpha}_i/H \gg \beta_i \gg |\dot{\beta}_i|/H$  with  $\dot{\beta}_i/H = -G [2\pi^2 m_i^2 T_\nu^2 + (56/15)\pi^4 T_\nu^4]$ . Comparing the  $\beta_i$  and  $\dot{\beta}_i$  terms,  $|\dot{\beta}_i|/\beta_i H \approx 2\pi^2 T_\nu^2/m_i^2 \lesssim 8 \times 10^{-5}$  which means it is safe to omit the  $\dot{\beta}_i$  terms. For convenience, the  $\dot{\alpha}_i$  terms in Eq. (C.3b) have been replaced by  $\alpha_i H$ .

The ensemble averages can now be replaced by the velocity ensemble averages,

$$\langle (\mathbf{v}_{\nu c} \cdot \hat{\mathbf{k}})^2 \rangle = \frac{1}{3} \int \frac{d|\mathbf{k}'|}{|\mathbf{k}'|} \Theta(|\mathbf{k}| - |\mathbf{k}'|) \left| \widetilde{W}(|\mathbf{k}'|R) \right|^2 \Delta_\zeta^2(\mathbf{k}') \left| \frac{T_{\theta_{\nu ic}}(\mathbf{k}', z)}{|\mathbf{k}'|} \right|^2, \quad (\text{C.4a})$$

$$\langle (\mathbf{v}_{\nu ic} \cdot \hat{\mathbf{k}}) [\partial_z (\mathbf{v}_{\nu ic} \cdot \hat{\mathbf{k}})] \rangle = \frac{1}{3} \int \frac{d|\mathbf{k}'|}{|\mathbf{k}'|} \Theta(|\mathbf{k}| - |\mathbf{k}'|) \left| \widetilde{W}(|\mathbf{k}'|R) \right|^2 \Delta_\zeta^2(\mathbf{k}') \left[ \frac{T_{\theta_{\nu ic}}}{|\mathbf{k}'|} \frac{\partial_z T_{\theta_{\nu ic}}}{|\mathbf{k}'|} \right], \quad (\text{C.4b})$$

$$\langle [\partial_z (\mathbf{v}_{\nu ic} \cdot \hat{\mathbf{k}})]^2 \rangle = \frac{1}{3} \int \frac{d|\mathbf{k}'|}{|\mathbf{k}'|} \Theta(|\mathbf{k}| - |\mathbf{k}'|) \left| \widetilde{W}(|\mathbf{k}'|R) \right|^2 \Delta_\zeta^2(\mathbf{k}') \left[ \frac{\partial_z T_{\theta_{\nu ic}}}{|\mathbf{k}'|} \right]^2, \quad (\text{C.4c})$$

where the relative transfer function  $T_{\theta_{\nu ic}} \equiv T_{\theta_{\nu i}} - T_{\theta_c}$  is defined as the difference between the C $\nu$ F and DM ones. The Heaviside- $\Theta$  function appears here to extract only the large scale modes ( $|\mathbf{k}| \rightarrow 0$ ) that can contribute coherently while those small scale modes are averaged out [73]. As shown in Fig. 3, the largest SNR happens in the region of  $k < 0.1 h/\text{Mpc}$  where the C $\nu$ B-DM power spectrum predicted by the linear theory receives little suppression compared to the  $N$ -body simulation [142]. Hence, our estimation based on the linear theory is also safe.

## References

- [1] W. Pauli, “*On the Earlier and more recent history of the neutrino,*” pages 193-217 of “*Writings on Physics and Philosophy*”, 978-3-54-056859-9, 978-0-387-56859-1, 978-3-64-208163-7, 978-3-66-202994-7, Springer-Verlag, January 1994.
- [2] W. F. Hornyak, T. Lauritsen, P. Morrison, and W. A. Fowler, “*Energy levels of light nuclei. iii,*” *Rev. Mod. Phys.* **22** (Oct, 1950) 291–372.
- [3] L. Langer and R. Moffat, “*The beta-spectrum of tritium and the mass of the neutrino,*” *Phys. Rev.* **88** no. 4, (1952) 689.
- [4] J. A. Formaggio, A. L. C. de Gouvêa, and R. G. H. Robertson, “*Direct Measurements of Neutrino Mass,*” *Phys. Rept.* **914** (2021) 1–54, [arXiv:2102.00594 [nucl-ex]].
- [5] **KATRIN** Collaboration, A. Osipowicz et al., “*KATRIN: A Next generation tritium beta decay experiment with sub-eV sensitivity for the electron neutrino mass. Letter of intent,*” [arXiv:hep-ex/0109033].

- [6] **KATRIN** Collaboration, M. Aker et al., “*Direct neutrino-mass measurement with sub-electronvolt sensitivity*,” *Nature Phys.* **18** no. 2, (2022) 160–166, [[arXiv:2105.08533](#) [hep-ex]].
- [7] **Particle Data Group** Collaboration, R. L. Workman et al., “*Review of Particle Physics*,” *PTEP* **2022** (2022) 083C01.
- [8] **KATRIN** Collaboration, J. Angrik et al., “*KATRIN design report 2004*,”.
- [9] **Super-Kamiokande** Collaboration, Y. Fukuda et al., “*Evidence for oscillation of atmospheric neutrinos*,” *Phys. Rev. Lett.* **81** (1998) 1562–1567, [[arXiv:hep-ex/9807003](#)].
- [10] **SNO** Collaboration, Q. R. Ahmad et al., “*Direct evidence for neutrino flavor transformation from neutral current interactions in the Sudbury Neutrino Observatory*,” *Phys. Rev. Lett.* **89** (2002) 011301, [[arXiv:nucl-ex/0204008](#)].
- [11] Shao-Feng Ge and Stephen J. Parke, “*Scalar Nonstandard Interactions in Neutrino Oscillation*,” *Phys. Rev. Lett.* **122**, no.21, 211801 (2019) [[arXiv:1812.08376](#) [hep-ph]].
- [12] Shao-Feng Ge and Hitoshi Murayama, “*Apparent CPT Violation in Neutrino Oscillation from Dark Non-Standard Interactions*,” [[arXiv:1904.02518](#) [hep-ph]]; Shao-Feng Ge, “*The Leptonic CP Measurement and New Physics Alternatives*,” *PoS NuFact2019*, 108 (2020) ([slides](#)); Shao-Feng Ge, “*New Physics with Scalar and Dark Non-Standard Interactions in Neutrino Oscillation*,” *J. Phys. Conf. Ser.* **1468**, no.1, 012125 (2020).
- [13] K. Y. Choi, E. J. Chun and J. Kim, “*Neutrino Oscillations in Dark Matter*,” *Phys. Dark Univ.* **30**, 100606 (2020) [[arXiv:1909.10478](#) [hep-ph]].
- [14] K. Y. Choi, E. J. Chun and J. Kim, “*Dispersion of neutrinos in a medium*,” [[arXiv:2012.09474](#) [hep-ph]].
- [15] M. Sen and A. Y. Smirnov, “*Refractive neutrino masses, ultralight dark matter and cosmology*,” [[arXiv:2306.15718](#) [hep-ph]].
- [16] P. F. de Salas, D. V. Forero, C. A. Ternes, M. Tortola, and J. W. F. Valle, “*Status of neutrino oscillations 2018:  $3\sigma$  hint for normal mass ordering and improved CP sensitivity*,” *Phys. Lett. B* **782** (2018) 633–640, [[arXiv:1708.01186](#) [hep-ph]].
- [17] F. Capozzi, E. Lisi, A. Marrone, and A. Palazzo, “*Current unknowns in the three neutrino framework*,” *Prog. Part. Nucl. Phys.* **102** (2018) 48–72, [[arXiv:1804.09678](#) [hep-ph]].
- [18] I. Esteban, M. C. Gonzalez-Garcia, M. Maltoni, T. Schwetz, and A. Zhou, “*The fate of hints: updated global analysis of three-flavor neutrino oscillations*,” *JHEP* **09** (2020) 178, [[arXiv:2007.14792](#) [hep-ph]].
- [19] **JUNO** Collaboration, F. An et al., “*Neutrino Physics with JUNO*,” *J. Phys. G* **43** no. 3, (2016) 030401, [[arXiv:1507.05613](#) [physics.ins-det]].

- [20] **JUNO** Collaboration, Z. Djurcic et al., “*JUNO Conceptual Design Report*,” [[arXiv:1508.07166](#) [physics.ins-det]].
- [21] S. T. Petcov and M. Piai, “*The LMA MSW solution of the solar neutrino problem, inverted neutrino mass hierarchy and reactor neutrino experiments*,” *Phys. Lett. B* **533** (2002) 94–106, [[arXiv:hep-ph/0112074](#)].
- [22] S. Choubey, S. T. Petcov, and M. Piai, “*Precision neutrino oscillation physics with an intermediate baseline reactor neutrino experiment*,” *Phys. Rev. D* **68** (2003) 113006, [[arXiv:hep-ph/0306017](#)].
- [23] J. Learned, S. T. Dye, S. Pakvasa, and R. C. Svoboda, “*Determination of neutrino mass hierarchy and  $\theta(13)$  with a remote detector of reactor antineutrinos*,” *Phys. Rev. D* **78** (2008) 071302, [[arXiv:hep-ex/0612022](#)].
- [24] L. Zhan, Y. Wang, J. Cao, and L. Wen, “*Determination of the Neutrino Mass Hierarchy at an Intermediate Baseline*,” *Phys. Rev. D* **78** (2008) 111103, [[arXiv:0807.3203](#) [hep-ex]].
- [25] L. Zhan, Y. Wang, J. Cao, and L. Wen, “*Experimental Requirements to Determine the Neutrino Mass Hierarchy Using Reactor Neutrinos*,” *Phys. Rev. D* **79** (2009) 073007, [[arXiv:0901.2976](#) [hep-ex]].
- [26] X. Qian, D. A. Dwyer, R. D. McKeown, P. Vogel, W. Wang, and C. Zhang, “*Mass Hierarchy Resolution in Reactor Anti-neutrino Experiments: Parameter Degeneracies and Detector Energy Response*,” *Phys. Rev. D* **87** no. 3, (2013) 033005, [[arXiv:1208.1551](#) [physics.ins-det]].
- [27] Shao-Feng Ge, K. Hagiwara, N. Okamura, and Y. Takaesu, “*Determination of mass hierarchy with medium baseline reactor neutrino experiments*,” *JHEP* **05** (2013) 131, [[arXiv:1210.8141](#) [hep-ph]].
- [28] X. Qian, A. Tan, W. Wang, J. J. Ling, R. D. McKeown, and C. Zhang, “*Statistical Evaluation of Experimental Determinations of Neutrino Mass Hierarchy*,” *Phys. Rev. D* **86** (2012) 113011, [[arXiv:1210.3651](#) [hep-ph]].
- [29] **JUNO** Collaboration, J. Zhang, “*JUNO Oscillation Physics*,” *J. Phys. Conf. Ser.* **2156** no. 1, (2021) 012110, [[arXiv:2111.10112](#) [physics.ins-det]].
- [30] W. H. Furry, “*On transition probabilities in double beta-disintegration*,” *Phys. Rev.* **56** (1939) 1184–1193.
- [31] M. Agostini, G. Benato, J. A. Detwiler, J. Menéndez, and F. Vissani, “*Toward the discovery of matter creation with neutrinoless  $\beta\beta$  decay*,” *Rev. Mod. Phys.* **95** no. 2, (2023) 025002, [[arXiv:2202.01787](#) [hep-ex]].
- [32] M. J. Dolinski, A. W. P. Poon, and W. Rodejohann, “*Neutrinoless Double-Beta Decay: Status and Prospects*,” *Ann. Rev. Nucl. Part. Sci.* **69** (2019) 219–251, [[arXiv:1902.04097](#) [nucl-ex]].

- [33] **KamLAND-Zen** Collaboration, A. Gando et al., “*Search for Majorana Neutrinos near the Inverted Mass Hierarchy Region with KamLAND-Zen*,” *Phys. Rev. Lett.* **117** no. 8, (2016) 082503, [arXiv:1605.02889 [hep-ex]]. [Addendum: *Phys.Rev.Lett.* 117, 109903 (2016)].
- [34] **GERDA** Collaboration, M. Agostini et al., “*Final Results of GERDA on the Search for Neutrinoless Double- $\beta$  Decay*,” *Phys. Rev. Lett.* **125** no. 25, (2020) 252502, [arXiv:2009.06079 [nucl-ex]].
- [35] Shao-Feng Ge and Werner Rodejohann, “*JUNO and Neutrinoless Double Beta Decay*,” *Phys. Rev. D* **92** no. 9, (2015) 093006, [arXiv:1507.05514 [hep-ph]].
- [36] Shao-Feng Ge and Manfred Lindner, “*Extracting Majorana properties from strong bounds on neutrinoless double beta decay*,” *Phys. Rev. D* **95** no. 3, (2017) 033003, [arXiv:1608.01618 [hep-ph]].
- [37] J. Cao, G.-Y. Huang, Y.-F. Li, Y. Wang, L.-J. Wen, Z.-Z. Xing, Z.-H. Zhao, and S. Zhou, “*Towards the meV limit of the effective neutrino mass in neutrinoless double-beta decays*,” *Chin. Phys. C* **44** no. 3, (2020) 031001, [arXiv:1908.08355 [hep-ph]].
- [38] Shao-Feng Ge and Jing-Yu Zhu, “*Phenomenological Advantages of the Normal Neutrino Mass Ordering*,” *Chin. Phys. C* **44** no. 8, (2020) 083103, [arXiv:1910.02666 [hep-ph]].
- [39] S. Dodelson and F. Schmidt, *Modern cosmology, second edition*. Academic press, 2020. ISBN: 978-0128159484.
- [40] B. Hernandez-Moliner, R. Jimenez, and C. Pena-Garay, “*Distinguishing Dirac vs. Majorana neutrinos: a cosmological probe*,” *JCAP* **08** no. 08, (2022) 038, [arXiv:2205.00808 [hep-ph]].
- [41] **PTOLEMY** Collaboration, E. Baracchini et al., “*PTOLEMY: A Proposal for Thermal Relic Detection of Massive Neutrinos and Directional Detection of MeV Dark Matter*,” [arXiv:1808.01892 [physics.ins-det]].
- [42] **PTOLEMY** Collaboration, M. G. Betti et al., “*Neutrino physics with the PTOLEMY project: active neutrino properties and the light sterile case*,” *JCAP* **07** (2019) 047, [arXiv:1902.05508 [astro-ph.CO]].
- [43] J. Alvey, M. Escudero, N. Sabti, and T. Schwetz, “*Cosmic neutrino background detection in large-neutrino-mass cosmologies*,” *Phys. Rev. D* **105** no. 6, (2022) 063501, [arXiv:2111.14870 [hep-ph]].
- [44] V. A. S. V. Bittencourt, A. E. Bernardini and M. Blasone, “*Chiral oscillations in the non-relativistic regime*,” *Eur. Phys. J. C* **81**, no.5, 411 (2021) [arXiv:2009.00084 [hep-ph]].
- [45] Shao-Feng Ge and Pedro Pasquini, “*Parity violation and chiral oscillation of cosmological relic neutrinos*,” *Phys. Lett. B* **811**, 135961 (2020) [arXiv:2009.01684 [hep-ph]].

- [46] M. Yoshimura, “*Neutrino Pair Emission from Excited Atoms*,” *Phys. Rev. D* **75**, 113007 (2007) [[arXiv:hep-ph/0611362](#) [hep-ph]].
- [47] A. Fukumi, S. Kuma, Y. Miyamoto, K. Nakajima, I. Nakano, H. Nanjo, C. Ohae, N. Sasao, M. Tanaka and T. Taniguchi, *et al.* “*Neutrino Spectroscopy with Atoms and Molecules*,” *PTEP* **2012**, 04D002 (2012) [[arXiv:1211.4904](#) [hep-ph]].
- [48] T. Hiraki, H. Hara, Y. Miyamoto, K. Imamura, T. Masuda, N. Sasao, S. Uetake, A. Yoshimi, K. Yoshimura and M. Yoshimura, “*Coherent two-photon emission from hydrogen molecules excited by counter-propagating laser pulses*,” *J. Phys. B* **52**, no.4, 045401 (2019) [[arXiv:1806.04005](#) [physics.atom-ph]].
- [49] M. Tashiro, B. P. Das, J. Ekman, P. Jönsson, N. Sasao and M. Yoshimura, “*Macro-coherent radiative emission of neutrino pair between parity-even atomic states*,” *Eur. Phys. J. C* **79**, no.11, 907 (2019) [[arXiv:1911.01639](#) [hep-ph]].
- [50] M. Yoshimura, “*Solitons and Precision Neutrino Mass Spectroscopy*,” *Phys. Lett. B* **699**, 123-128 (2011) [[arXiv:1101.2749](#) [hep-ph]].
- [51] M. Yoshimura, N. Sasao and M. Tanaka, “*Dynamics of paired superradiance*,” *Phys. Rev. A* **86**, 013812 (2012) [[arXiv:1203.5394](#) [quant-ph]].
- [52] Shao-Feng Ge and Pedro Pasquini, “*Probing light mediators in the radiative emission of neutrino pair*,” *Eur. Phys. J. C* **82**, no.3, 208 (2022) [[arXiv:2110.03510](#) [hep-ph]].
- [53] Shao-Feng Ge and Pedro Pasquini, “*Unique probe of neutrino electromagnetic moments with radiative pair emission*,” *Phys. Lett. B* **841**, 137911 (2023) [[arXiv:2206.11717](#) [hep-ph]].
- [54] Shao-Feng Ge and Pedro Pasquini, “*Disentangle Neutrino Electromagnetic Properties with Atomic Radiative Pair Emission*,” [[arXiv:2306.12953](#) [hep-ph]].
- [55] M. Yoshimura, A. Fukumi, N. Sasao and T. Yamaguchi, “*Parity violating observables in radiative neutrino pair emission from metastable atoms*,” *Prog. Theor. Phys.* **123**, 523-532 (2010) [[arXiv:0907.0519](#) [hep-ph]].
- [56] D. N. Dinh, S. T. Petcov, N. Sasao, M. Tanaka, and M. Yoshimura, “*Observables in Neutrino Mass Spectroscopy Using Atoms*,” *Phys. Lett. B* **719** (2013) 154–163, [[arXiv:1209.4808](#) [hep-ph]].
- [57] N. Song, R. Boyero Garcia, J. J. Gomez-Cadenas, M. C. Gonzalez-Garcia, A. Peralta Conde, and J. Taron, “*Conditions for Statistical Determination of the Neutrino Mass Spectrum in Radiative Emission of Neutrino Pairs in Atoms*,” *Phys. Rev. D* **93** no. 1, (2016) 013020, [[arXiv:1510.00421](#) [hep-ph]].
- [58] J. Zhang and S. Zhou, “*Improved Statistical Determination of Absolute Neutrino Masses via Radiative Emission of Neutrino Pairs from Atoms*,” *Phys. Rev. D* **93** no. 11, (2016) 113020, [[arXiv:1604.08008](#) [hep-ph]].

- [59] G. T. Zatsepin, “*On the possibility of determining the upper limit of the neutrino mass by means of the flight time,*” *Pisma Zh. Eksp. Teor. Fiz.* **8** (1968) 333–334.
- [60] **Hyper-Kamiokande** Collaboration, K. Abe et al., “*Hyper-Kamiokande Design Report,*” [[arXiv:1805.04163](#) [physics.ins-det]].
- [61] T. J. Loredo and D. Q. Lamb, “*Bayesian analysis of neutrinos observed from supernova SN-1987A,*” *Phys. Rev. D* **65** (2002) 063002, [[arXiv:astro-ph/0107260](#)].
- [62] J.-S. Lu, J. Cao, Y.-F. Li, and S. Zhou, “*Constraining Absolute Neutrino Masses via Detection of Galactic Supernova Neutrinos at JUNO,*” *JCAP* **05** (2015) 044, [[arXiv:1412.7418](#) [hep-ph]].
- [63] F. Pompa, F. Capozzi, O. Mena, and M. Sorel, “*Absolute  $\nu$  Mass Measurement with the DUNE Experiment,*” *Phys. Rev. Lett.* **129** no. 12, (2022) 121802, [[arXiv:2203.00024](#) [hep-ph]].
- [64] J. Lesgourgues and S. Pastor, “*Massive neutrinos and cosmology,*” *Phys. Rept.* **429** (2006) 307–379, [[arXiv:astro-ph/0603494](#)].
- [65] A. Boyle and E. Komatsu, “*Deconstructing the neutrino mass constraint from galaxy redshift surveys,*” *JCAP* **03** (2018) 035, [[arXiv:1712.01857](#) [astro-ph.CO]].
- [66] M. Lattanzi and M. Gerbino, “*Status of neutrino properties and future prospects - Cosmological and astrophysical constraints,*” *Front. in Phys.* **5** (2018) 70, [[arXiv:1712.07109](#) [astro-ph.CO]].
- [67] **Planck** Collaboration, N. Aghanim et al., “*Planck 2018 results. VI. Cosmological parameters,*” *Astron. Astrophys.* **641** (2020) A6, [[arXiv:1807.06209](#) [astro-ph.CO]]. [Erratum: *Astron. Astrophys.* 652, C4 (2021)].
- [68] **DES** Collaboration, T. M. C. Abbott et al., “*Dark Energy Survey Year 3 results: Cosmological constraints from galaxy clustering and weak lensing,*” *Phys. Rev. D* **105** no. 2, (2022) 023520, [[arXiv:2105.13549](#) [astro-ph.CO]].
- [69] M. Kaplinghat, L. Knox and Y. S. Song, “*Determining neutrino mass from the CMB alone,*” *Phys. Rev. Lett.* **91**, 241301 (2003) [[arXiv:astro-ph/0303344](#) [astro-ph]].
- [70] S. C. Hotinli, N. Sabti, J. North and M. Kamionkowski, “*Unveiling neutrino halos with CMB lensing,*” *Phys. Rev. D* **108**, no.10, 103504 (2023) [[arXiv:2306.15715](#) [astro-ph.CO]].
- [71] H. M. Zhu, U. L. Pen, X. Chen and D. Inman, “*Probing Neutrino Hierarchy and Chirality via Wakes,*” *Phys. Rev. Lett.* **116**, no.14, 141301 (2016) [[arXiv:1412.1660](#) [astro-ph.CO]].
- [72] H.-M. Zhu, U.-L. Pen, X. Chen, D. Inman, and Y. Yu, “*Measurement of Neutrino Masses from Relative Velocities,*” *Phys. Rev. Lett.* **113** (2014) 131301, [[arXiv:1311.3422](#) [astro-ph.CO]].



- [73] C. Okoli, M. I. Scrimgeour, N. Afshordi, and M. J. Hudson, “*Dynamical friction in the primordial neutrino sea*,” *Mon. Not. Roy. Astron. Soc.* **468** no. 2, (2017) 2164–2175, [[arXiv:1611.04589](#) [astro-ph.CO]].
- [74] H. M. Zhu and E. Castorina, “Measuring dark matter-neutrino relative velocity on cosmological scales,” *Phys. Rev. D* **101**, no.2, 023525 (2020) [[arXiv:1905.00361](#) [astro-ph.CO]].
- [75] C. Nascimento and M. Loverde, “Neutrino winds on the sky,” *JCAP* **11**, 036 (2023) [[arXiv:2307.00049](#) [astro-ph.CO]].
- [76] **DESI** Collaboration, A. Aghamousa et al., “*The DESI Experiment Part I: Science, Targeting, and Survey Design*,” [[arXiv:1611.00036](#) [astro-ph.IM]].
- [77] **DESI** Collaboration, A. Dey et al., “*Overview of the DESI Legacy Imaging Surveys*,” *Astron. J.* **157** no. 5, (2019) 168, [[arXiv:1804.08657](#) [astro-ph.IM]].
- [78] **DESI** Collaboration, G. Adame et al., “*The Early Data Release of the Dark Energy Spectroscopic Instrument*,” [[arXiv:2306.06308](#) [astro-ph.CO]].
- [79] **EUCLID** Collaboration, R. Laureijs et al., “*Euclid Definition Study Report*,” [[arXiv:1110.3193](#) [astro-ph.CO]].
- [80] Y. Cao et al., “*Testing photometric redshift measurements with filter definition of the chinese space station optical survey (css-os)*,” *Mon. Not. Roy. Astron. Soc.* **480** no. 2, (2018) 2178–2190.
- [81] Y. Cao, Y. Gong, D. Liu, A. Cooray, C. Feng, and X. Chen, “*Anisotropies of cosmic optical and near-ir background from the china space station telescope (csst)*,” *Mon. Not. Roy. Astron. Soc.* **511** no. 2, (2022) 1830–1840.
- [82] Y. Cao, Y. Gong, Z.-Y. Zheng, and C. Xu, “*Calibrating photometric redshift measurements with the multi-channel imager (mci) of the china space station telescope (csst)*,” *Res. Astron. Astrophys.* **22** no. 2, (2022) 025019.
- [83] Scott Dodelson, “*Gravitational Lensing*,” June 2017, Cambridge: Cambridge University Press, Hardcopy ISBN: 9781107129764, eBook ISBN 9781316424254.
- [84] Arthur B. Congdon and Charles R. Keeton, “*Principles of Gravitational Lensing: Light Deflection as a Probe of Astrophysics and Cosmology*,” December 2018, Springer Praxis Books, Hardcover ISBN 978-3-030-02121-4, eBook ISBN 978-3-030-02122-1.
- [85] Massimo Meneghetti, “*Introduction to Gravitational Lensing With Python Examples*,” Lecture Notes in Physics Vol. 956, Springer, Hardcopy ISBN 978-3-030-73581-4, eBook ISBN 978-3-030-73582-1.
- [86] K. Griest, “*Effect of the Sun’s Gravity on the Distribution and Detection of Dark Matter Near the Earth*,” *Phys. Rev. D* **37**, 2703 (1988).



- [87] P. Sikivie and S. Wick, “*Solar wakes of dark matter flows,*” *Phys. Rev. D* **66**, 023504 (2002) [[arXiv:astro-ph/0203448](#) [astro-ph]].
- [88] S. K. Lee, M. Lisanti, A. H. G. Peter and B. R. Safdi, “*Effect of Gravitational Focusing on Annual Modulation in Dark-Matter Direct-Detection Experiments,*” *Phys. Rev. Lett.* **112**, no.1, 011301 (2014) [[arXiv:1308.1953](#) [astro-ph.CO]].
- [89] N. Bozorgnia and T. Schwetz, “*Is the effect of the Sun’s gravitational potential on dark matter particles observable?,*” *JCAP* **08**, 013 (2014) [[arXiv:1405.2340](#) [astro-ph.CO]].
- [90] S. Chandrasekhar, “*Dynamical Friction. I. General Considerations: the Coefficient of Dynamical Friction.,*” *Astrophys.J.* **97** (Mar., 1943) 255.
- [91] D. P. O’Brien, A. Morbidelli, and H. F. Levison, “*Terrestrial planet formation with strong dynamical friction,*” *Icarus* **184** no. 1, (Sept., 2006) 39–58.
- [92] S. S. Kim and M. Morris, “*Dynamical Friction on Star Clusters near the Galactic Center,*” *Astrophys.J.* **597** no. 1, (Nov., 2003) 312–322, [[arXiv:astro-ph/0307271](#) [astro-ph]].
- [93] C. Struck, “*Galaxy collisions.,*” *Phys.Rept.* **321** (Jan., 1999) 1–137, [[arXiv:astro-ph/9908269](#) [astro-ph]].
- [94] S. Weinberg, *The Quantum theory of fields. Vol. 1: Foundations.* Cambridge University Press, 6, 2005. Chapter 3.1.
- [95] M. LoVerde, “*Halo bias in mixed dark matter cosmologies,*” *Phys. Rev. D* **90** no. 8, (2014) 083530, [[arXiv:1405.4855](#) [astro-ph.CO]].
- [96] M. S. Alenazi and P. Gondolo, “*Phase-space distribution of unbound dark matter near the Sun,*” *Phys. Rev. D* **74**, 083518 (2006) [[arXiv:astro-ph/0608390](#) [astro-ph]].
- [97] F. Bernardeau, S. Colombi, E. Gaztanaga and R. Scoccimarro, “*Large scale structure of the universe and cosmological perturbation theory,*” *Phys. Rept.* **367** (2002), 1-248 [[arXiv:astro-ph/0112551](#) [astro-ph.CO]].
- [98] P. McDonald, “*Gravitational redshift and other redshift-space distortions of the imaginary part of the power spectrum,*” *JCAP* **11** (2009) 026, [[arXiv:0907.5220](#) [astro-ph.CO]].
- [99] D. Tseliakhovich and C. Hirata, “*Relative velocity of dark matter and baryonic fluids and the formation of the first structures,*” *Phys. Rev. D* **82** (2010) 083520, [[arXiv:1005.2416](#) [astro-ph.CO]].
- [100] J. Yoo and U. Seljak, “*Signatures of first stars in galaxy surveys: Multitracer analysis of the supersonic relative velocity effect and the constraints from the BOSS power spectrum measurements,*” *Phys. Rev. D* **88** no. 10, (2013) 103520, [[arXiv:1308.1401](#) [astro-ph.CO]].
- [101] D. Inman, H. R. Yu, H. M. Zhu, J. D. Emberson, U. L. Pen, T. J. Zhang, S. Yuan, X. Chen and Z. Z. Xing, “*Simulating the cold dark matter-neutrino dipole with TianNu,*” *Phys. Rev. D* **95**, no.8, 083518 (2017) [[arXiv:1610.09354](#) [astro-ph.CO]].

- [102] C.-T. Chiang, C. Wagner, F. Schmidt, and E. Komatsu, “*Position-dependent power spectrum of the large-scale structure: a novel method to measure the squeezed-limit bispectrum*,” *JCAP* **05** (2014) 048, [[arXiv:1403.3411](#) [astro-ph.CO]].
- [103] C. Wagner, F. Schmidt, C.-T. Chiang, and E. Komatsu, “*Separate Universe Simulations*,” *Mon. Not. Roy. Astron. Soc.* **448** no. 1, (2015) L11–L15, [[arXiv:1409.6294](#) [astro-ph.CO]].
- [104] C. Wagner, F. Schmidt, C.-T. Chiang, and E. Komatsu, “*The angle-averaged squeezed limit of nonlinear matter  $N$ -point functions*,” *JCAP* **08** (2015) 042, [[arXiv:1503.03487](#) [astro-ph.CO]].
- [105] A. Smith, S. Cole, C. Baugh, Z. Zheng, R. Angulo, P. Norberg, and I. Zehavi, “*A Lightcone Catalogue from the Millennium-XXL Simulation*,” *Mon. Not. Roy. Astron. Soc.* **470** no. 4, (2017) 4646–4661, [[arXiv:1701.06581](#) [astro-ph.CO]].
- [106] A. Smith, S. Cole, C. Grove, P. Norberg, and P. Zarrouk, “*A light-cone catalogue from the Millennium-XXL simulation: improved spatial interpolation and colour distributions for the DESI BGS*,” *Mon. Not. Roy. Astron. Soc.* **516** no. 3, (2022) 4529–4542, [[arXiv:2207.04902](#) [astro-ph.CO]].
- [107] W. H. Press and P. Schechter, “*Formation of galaxies and clusters of galaxies by selfsimilar gravitational condensation*,” *Astrophys. J.* **187**, 425–438 (1974)
- [108] H. Mo, F. C. van den Bosch, and S. White, *Galaxy Formation and Evolution*. Cambridge University Press, 2010.
- [109] A. V. Kravtsov, A. A. Berlind, R. H. Wechsler, A. A. Klypin, S. Gottloeber, B. Allgood, and J. R. Primack, “*The Dark side of the halo occupation distribution*,” *Astrophys. J.* **609** (2004) 35–49, [[arXiv:astro-ph/0308519](#)].
- [110] S. Murray, C. Power, and A. S. G. Robotham, “*HMFcalc: An online tool for calculating dark matter halo mass functions*,” *Astron. Comput.* **3-4** (2013) 23–34, [[arXiv:1306.6721](#) [astro-ph.CO]].
- [111] S. G. Murray, B. Diemer, Z. Chen, A. G. Neuhold, M. A. Schnapp, T. Peruzzi, D. Blevins, and T. Engelman, “*TheHaloMod: An online calculator for the halo model*,” *Astron. Comput.* **36** (2021) 100487, [[arXiv:2009.14066](#) [astro-ph.CO]].
- [112] R. K. Sheth, H. J. Mo, and G. Tormen, “*Ellipsoidal collapse and an improved model for the number and spatial distribution of dark matter haloes*,” *Mon. Not. Roy. Astron. Soc.* **323** (2001) 1, [[arXiv:astro-ph/9907024](#)].
- [113] SDSS Collaboration, I. Zehavi et al., “*Galaxy Clustering in the Completed SDSS Redshift Survey: The Dependence on Color and Luminosity*,” *Astrophys. J.* **736** (2011) 59–88, [[arXiv:1005.2413](#) [astro-ph.CO]].
- [114] P. Schechter, “*An analytic expression for the luminosity function for galaxies*,” *Astrophys. J.* **203** (1976) 297–306.

- [115] J. Loveday et al., “*Galaxy and Mass Assembly (GAMA): ugriz galaxy luminosity functions*,” *Mon. Not. Roy. Astron. Soc.* **420** (2011) 1239–1262, [[arXiv:1111.0166](#) [astro-ph.CO]].
- [116] SDSS Collaboration, M. R. Blanton et al., “*The Galaxy luminosity function and luminosity density at redshift  $z = 0.1$* ” *Astrophys. J.* **592** (2003) 819–838, [[arXiv:astro-ph/0210215](#)].
- [117] D. Ginzburg and V. Desjacques, “*Shot noise in multitracer constraints on  $fNL$  and relativistic projections: Power spectrum*,” *Mon. Not. Roy. Astron. Soc.* **495**, no.1, 932-942 (2020) [[arXiv:1911.11701](#) [astro-ph.CO]].
- [118] R. K. Sheth and G. Tormen, “*Large scale bias and the peak background split*,” *Mon. Not. Roy. Astron. Soc.* **308** (1999) 119, [[arXiv:astro-ph/9901122](#)].
- [119] A. Vale and J. P. Ostriker, “*Linking halo mass to galaxy luminosity*,” *Mon. Not. Roy. Astron. Soc.* **353**, 189 (2004) [[arXiv:astro-ph/0402500](#) [astro-ph]].
- [120] X. H. Yang, H. J. Mo, Y. P. Jing and F. C. van den Bosch, “*Galaxy occupation statistics of dark matter haloes: Observational results*,” *Mon. Not. Roy. Astron. Soc.* **358**, 217-232 (2005) [[arXiv:astro-ph/0410114](#) [astro-ph]].
- [121] X. Yang, H. J. Mo, F. C. v. d. Bosch, A. Pasquali, C. Li, and M. Barden, “*Galaxy Groups in the SDSS DR4: I. The Catalogue and Basic Properties*,” *Astrophys. J.* **671** (2007) 153–170, [[arXiv:0707.4640](#) [astro-ph]].
- [122] X. Yang et al., “*An Extended Halo-based Group/Cluster finder: application to the DESI legacy imaging surveys DR8*,” *Astrophys. J.* **909** no. 2, (2021) 143, [[arXiv:2012.14998](#) [astro-ph.GA]].
- [123] V. Desjacques, D. Jeong and F. Schmidt, “*Large-Scale Galaxy Bias*,” *Phys. Rept.* **733**, 1-193 (2018) [[arXiv:1611.09787](#) [astro-ph.CO]].
- [124] N. Mostek, A. L. Coil, M. Cooper, M. Davis, J. A. Newman, and B. J. Weiner, “*The deep2 galaxy redshift survey: Clustering dependence on galaxy stellar mass and star formation rate at  $z \sim 1$* ,” *The Astrophysical Journal* **767** no. 1, (Mar., 2013) 89, [[arXiv:1210.6694](#) [astro-ph.CO]].
- [125] N. P. Ross, Y. Shen, M. A. Strauss, D. E. Vanden Berk, A. J. Connolly, G. T. Richards, D. P. Schneider, D. H. Weinberg, P. B. Hall, N. A. Bahcall, and R. J. Brunner, “*Clustering of low-redshift ( $z \leq 2.2$ ) quasars from the sloan digital sky survey*,” *The Astrophysical Journal* **697** no. 2, (May, 2009) 1634–1655, [[arXiv:0903.3230](#) [astro-ph.CO]].
- [126] H. Zhan, “*Consideration for a large-scale multi-color imaging and slitless spectroscopy survey on the Chinese space station and its application in dark energy research*,” *Scientia Sinica Physica, Mechanica & Astronomica* **41** no. 12, (Jan., 2011) 1441.
- [127] Y. Cao, Y. Gong, X.-M. Meng, C. K. Xu, X. Chen, Q. Guo, R. Li, D. Liu, Y. Xue, L. Cao, X. Fu, X. Zhang, S. Wang, and H. Zhan, “*Testing photometric redshift measurements with*

- filter definition of the Chinese Space Station Optical Survey (CSS-OS),* *Mon. Not. Roy. Astron. Soc.* **480** no. 2, (Oct., 2018) 2178–2190, [[arXiv:1706.09586](#) [astro-ph.IM]].
- [128] Y. Gong, X. Liu, Y. Cao, X. Chen, Z. Fan, R. Li, X.-D. Li, Z. Li, X. Zhang, and H. Zhan, “*Cosmology from the Chinese Space Station Optical Survey (CSS-OS),*” *Astrophys. J.* **883** (2019) 203, [[arXiv:1901.04634](#) [astro-ph.CO]].
- [129] A. Chen, Y. Gong, F. Wu, Y. Wang, and X. Chen, “*Constraining Brans–Dicke Cosmology with the CSST Galaxy Clustering Spectroscopic Survey,*” *Res. Astron. Astrophys.* **22** no. 5, (2022) 055021, [[arXiv:2202.07571](#) [astro-ph.CO]].
- [130] H. Lin, Y. Gong, X. Chen, K. C. Chan, Z. Fan, and H. Zhan, “*Forecast of neutrino cosmology from the CSST photometric galaxy clustering and cosmic shear surveys,*” *Mon. Not. Roy. Astron. Soc.* **515** no. 4, (2022) 5743–5757, [[arXiv:2203.11429](#) [astro-ph.CO]].
- [131] **DESI** Collaboration, D. J. Schlegel et al., “*A Spectroscopic Road Map for Cosmic Frontier: DESI, DESI-II, Stage-5,*” [[arXiv:2209.03585](#) [astro-ph.CO]].
- [132] T. Sunayama, “*Subaru PFS Cosmology,*” *Kashiwa Dark Matter Symposium 2023*.
- [133] L. Amendola et al., “*Cosmology and fundamental physics with the Euclid satellite,*” *Living Rev. Rel.* **21** no. 1, (2018) 2, [[arXiv:1606.00180](#) [astro-ph.CO]].
- [134] C. Carbone, L. Verde, Y. Wang, and A. Cimatti, “*Neutrino constraints from future nearly all-sky spectroscopic galaxy surveys,*” *JCAP* **2011** no. 03, (Mar., 2011) 030–030, [[arXiv:1012.2868](#) [astro-ph.CO]].
- [135] J. Lesgourgues, S. Pastor and L. Perotto, “*Probing neutrino masses with future galaxy redshift surveys,*” *Phys. Rev. D* **70**, 045016 (2004) [[arXiv:hep-ph/0403296](#) [hep-ph]].
- [136] D. Blas, J. Lesgourgues, and T. Tram, “*The Cosmic Linear Anisotropy Solving System (CLASS) II: Approximation schemes,*” *JCAP* **07** (2011) 034, [[arXiv:1104.2933](#) [astro-ph.CO]].
- [137] Y. Wu, W. Xiao, R. Mu, D. Batuski, and A. Khalil, “*Nearest neighbor vector analysis of sdss DR5 galaxy distribution,*” *Natural Science*, **5**, 47-51., [[arXiv:1212.1671](#) [astro-ph.CO]].
- [138] C.-P. Ma and E. Bertschinger, “*Cosmological perturbation theory in the synchronous and conformal newtonian gauges,*” *Astrophys. J.* **455** (Dec., 1995) 7. [[arXiv:astro-ph/9401007](#) [astro-ph]].
- [139] C. Howlett, A. Lewis, A. Hall and A. Challinor, “*CMB power spectrum parameter degeneracies in the era of precision cosmology,*” *JCAP* **04** (2012), 027 [[arXiv:1201.3654](#) [astro-ph.CO]].
- [140] M. Doran, “*CMBEASY: an object oriented code for the cosmic microwave background,*” *JCAP* **10** (2005), 011 [[arXiv:astro-ph/0302138](#) [astro-ph.CO]].

- [141] M. Zaldarriaga, U. Seljak and E. Bertschinger, “*Integral solution for the microwave background anisotropies in nonflat universes,*” *Astrophys. J.* **494** (1998), 491-502 [[arXiv:astro-ph/9704265](#) [astro-ph.CO]].
- [142] D. Inman, J. D. Emberson, U.-L. Pen, A. Farchi, H.-R. Yu, and J. Harnois-Déraps, “*Precision reconstruction of the cold dark matter-neutrino relative velocity from N-body simulations,*” *Phys. Rev. D* **92** no. 2, (2015) 023502, [[arXiv:1503.07480](#) [astro-ph.CO]].